

1 Barium and carbon fluxes in the Canadian Arctic Archipelago

2 Helmuth Thomas,¹ Elizabeth Shadwick,^{1,2} Frank Dehairs,³ Bruno Lansard,⁴
 3 Alfonso Mucci,⁴ Jacques Navez,³ Yves Gratton,⁵ Friederike Prowe,⁶ Melissa Chierici,⁷
 4 Agneta Fransson,⁸ Tim N. Papakyriakou,⁹ Erika Sternberg,¹ Lisa A. Miller,¹⁰
 5 Jean-Éric Tremblay,¹¹ and Christophe Monnin¹²

6 Received 9 March 2011; revised 3 August 2011; accepted 8 September 2011; published XX Month 2011.

7 [1] The seasonal and spatial variability of dissolved Barium (Ba) in the Amundsen Gulf,
 8 southeastern Beaufort Sea, was monitored over a full year from September 2007 to
 9 September 2008. Dissolved Ba displays a nutrient-type behavior: the maximum water
 10 column concentration is located below the surface layer. The highest Ba concentrations
 11 are typically observed at river mouths, the lowest concentrations are found in water
 12 masses of Atlantic origin. Barium concentrations decrease eastward through the Canadian
 13 Arctic Archipelago. Barite (BaSO₄) saturation is reached at the maximum dissolved
 14 Ba concentrations in the subsurface layer, whereas the rest of the water column is
 15 undersaturated. A three end-member mixing model comprising freshwater from sea-ice
 16 melt and rivers, as well as upper halocline water, is used to establish their relative
 17 contributions to the Ba concentrations in the upper water column of the Amundsen
 18 Gulf. Based on water column and riverine Ba contributions, we assess the depletion of
 19 dissolved Ba by formation and sinking of biologically bound Ba (bio-Ba), from which
 20 we derive an estimate of the carbon export production. In the upper 50 m of the water
 21 column of the Amundsen Gulf, riverine Ba accounts for up to 15% of the available
 22 dissolved Ba inventory, of which up to 20% is depleted by bio-Ba formation and export.
 23 Since riverine inputs and Ba export occur concurrently, the seasonal variability of
 24 dissolved Ba in the upper water column is moderate. Assuming a fixed organic carbon to
 25 bio-Ba flux ratio, carbon export out of the surface layer is estimated at $1.8 \pm 0.45 \text{ mol C}$
 26 $\text{m}^{-2} \text{ yr}^{-1}$. Finally, we propose a climatological carbon budget for the Amundsen Gulf
 27 based on recent literature data and our findings, the latter bridging the surface and
 28 subsurface water carbon cycles.

29 **Citation:** Thomas, H., et al. (2011), Barium and carbon fluxes in the Canadian Arctic Archipelago, *J. Geophys. Res.*, 116,
 30 XXXXXX, doi:10.1029/2011JC007120.

¹Department of Oceanography, Dalhousie University, Halifax, Nova Scotia, Canada.

²Now at Antarctic Climate and Ecosystems Cooperative Research Center, Hobart, Tasmania, Australia.

³Earth System Sciences and Analytical and Environmental Chemistry, Vrije Universiteit Brussel, Brussels, Belgium.

⁴Department of Earth and Planetary Sciences, McGill University, Montreal, Quebec, Canada.

⁵INRS-ETE, Quebec, Quebec, Canada.

⁶Leibniz Institute of Marine Sciences at University of Kiel (IFM-GEOMAR), Kiel, Germany.

⁷Department of Chemistry, University of Gothenburg, Göteborg, Sweden.

⁸Department of Earth Sciences, University of Gothenburg, Göteborg, Sweden.

⁹Center for Earth Observation Science, University of Manitoba, Winnipeg, Manitoba, Canada.

¹⁰Institute of Ocean Sciences, Fisheries and Oceans Canada, Sidney, British Columbia, Canada.

¹¹Department de Biologie, Université Laval, Quebec, Quebec, Canada.

¹²Laboratoire Mécanismes et Transferts en Géologie, CNRS-Université Paul Sabatier, Toulouse, France.

1. Introduction

31

[2] Barium (Ba) has increasingly been employed as water mass tracer and as biogeochemical proxy of biological productivity. Here, we combine both approaches in order to gain insights into the biogeochemistry of Ba and its relationship to the inorganic carbon cycle in the Canadian Arctic Archipelago. Finally, we use dissolved Ba data to assess export production of organic carbon, which in turn enables us to balance the carbon budget for our investigation area.

[3] The strong correlation between the distributions of barium bound to particulate organic matter (bio-Ba) and particulate organic carbon (C_{org}) in the oceans and sediments has led to the use of bio-Ba as a proxy of biological productivity, in particular of export production from seasonal to geological time scales [e.g., Bishop, 1988; Dehairs et al., 1992, 1997; Dymond et al., 1992; Francois et al., 1995; Dymond and Collier, 1996; Gillikin et al., 2006; Sternberg et al., 2007; Calvert and Pederson, 2007]. As summarized by Sternberg et al. [2007], aggregates containing bio-Ba are formed in the upper water column. Accordingly, the highest

32
33
34
35
36
37
38
39
40
41
42
43
44
45
46
47
48
49
50

51 bio-Ba concentrations are typically observed in surface
 52 waters, although such maxima may be less accentuated or
 53 missing in certain regions or seasons. A subsurface maximum
 54 of bio-Ba is also often observed in the mesopelagic layer and
 55 primarily consists of barite (BaSO_4) micro-crystals [Bishop,
 56 1988; Dehairs et al., 1997; Jeandel et al., 2000; Jacquet
 57 et al., 2007; Sternberg et al., 2008; Dehairs et al., 2008].
 58 The presence of barite micro-crystals in oceanic suspended
 59 particulate matter is quite ubiquitous, despite the fact that most
 60 ocean waters are undersaturated with respect to this mineral
 61 [Monnin et al., 1999]. Several hypotheses have been proposed
 62 to explain this conundrum [e.g., Bishop, 1988; Dehairs et al.,
 63 1997; Sternberg et al., 2005, 2008; van Beek et al., 2009],
 64 most of which call upon biological processes including
 65 respiratory activity in the mesopelagic layer [Dehairs et al.,
 66 1992]. A detailed review of these hypotheses is discussed
 67 by Sternberg et al. [2007], and Jacquet et al. [2011] sum-
 68 marize these by reporting that barite precipitates in super-
 69 saturated microenvironments during the bacterial degradation
 70 of sinking organic matter. In other words, organic particles
 71 that escape breakdown during settling through the water col-
 72 umn accumulate barite, thus explaining the observed depth-
 73 dependent increase of Ba fluxes [e.g., Francois et al., 1995].
 74 [4] The continual formation of barite in biogenic aggre-
 75 gates, which settle through the water column, serves to increase
 76 Ba fluxes with depth and thus lowers the organic carbon to
 77 bio-Ba ($C_{\text{org}}:\text{bio-Ba}$) flux ratio with depth. Moreover, this
 78 ratio decreases with depth as a result of the (preferential)
 79 respiration of organic carbon relative to the release or dis-
 80 solution of bio-Ba. Such observations have been reported in
 81 several, but not all regions of the deep oceans [Dymond et al.,
 82 1992, Francois et al., 1995], and thus the $C_{\text{org}}:\text{bio-Ba}$ flux
 83 ratios recorded in ocean basins vary regionally [Dymond
 84 et al., 1992; Francois et al., 1995; Dymond and Collier,
 85 1996]. On the other hand, Dymond et al. [1992] and
 86 Francois et al. [1995] have shown that within the euphotic
 87 zone and irrespective of the ocean basin, the $C_{\text{org}}:\text{bio-Ba}$ flux
 88 ratio converges to a value of approximately $C_{\text{org}}:\text{bio-Ba} =$
 89 $200 \text{ g C (g Ba)}^{-1}$ [$2290 \text{ mol C (mol Ba)}^{-1}$], close to
 90 the globally estimated ratio $C_{\text{org}}:\text{bio-Ba} = 260 \text{ g C (g Ba)}^{-1}$
 91 [$2860 \text{ mol C (mol Ba)}^{-1}$] reported by Broecker and Peng
 92 [1982]. Higher $C_{\text{org}}:\text{bio-Ba}$ flux ratios have been observed
 93 in continental margins [Dehairs et al., 2000] and have been
 94 attributed to the formation of aggregates of both open ocean
 95 and margin carbon, and to differences in functioning of
 96 open ocean and marine ecosystems. Later in this paper,
 97 we exploit this fact to assess the export of marine carbon out
 98 of the euphotic zone, rather than an overall carbon export
 99 comprising terrestrial and marine carbon.

100 [5] It is difficult to quantitatively relate the behavior of
 101 particulate and dissolved Ba in the water column to each
 102 other, since, like Ca, dissolved Ba concentrations are 2–3
 103 orders of magnitude larger than those of particulate Ba [e.g.,
 104 Jacquet et al., 2005, 2007]. Dissolved Ba displays a nutrient-
 105 type profile, which is, as we later argue, primarily shaped by
 106 the generation of bio-Ba in the surface layer and the subse-
 107 quent release of Ba during the respiratory breakdown of the
 108 organic matter below the euphotic zone. In the mesopelagic
 109 and deep oceans, the formation and dissolution rates of barite
 110 (BaSO_4) also influence the vertical distributions and con-
 111 centrations of dissolved Ba. Dissolved Ba has been
 112 employed as a water mass tracer in various ocean basins,

including the Southern Ocean [e.g., Jacquet et al., 2005, 113
 2007; Hoppema et al., 2010], and has been most useful in 114
 the Arctic Ocean, since Arctic rivers draining the North 115
 American continent carry significantly higher dissolved Ba 116
 concentrations than their Eurasian counterparts [e.g., Cooper 117
 et al., 2008]. Few studies discuss factors that control the 118
 distribution of dissolved Ba in the water column of the Arctic 119
 region [e.g., Falkner et al., 1994; Guay and Falkner, 1997; 120
 Taylor et al., 2003; Guay et al., 2009]. Complemented by 121
 additional tracers, such as total alkalinity (A_T) or the stable 122
 oxygen isotope composition of seawater ($\delta^{18}\text{O}$), dissolved 123
 Ba has been used to determine the nature/origin and contri- 124
 bution of freshwater (sea-ice melt and river runoff) to Arctic 125
 Ocean surface waters [e.g., Falkner et al., 1994; Guay and 126
 Falkner, 1997, 1998; Cooper et al., 2008; Bates et al., 127
 2009; Yamamoto-Kawai et al., 2010]. In the surface 128
 waters, the concentrations of dissolved Ba reveal a high 129
 spatial variability with significantly enhanced concentrations 130
 of dissolved Ba close to the river mouths [e.g., Guay et al., 131
 2009; Yamamoto-Kawai et al., 2010]. Likewise, the strong 132
 seasonality of river runoff is reflected in the temporal vari- 133
 ability of the surface dissolved Ba concentrations in near- 134
 shore regions, a feature that has not been readily captured 135
 in recent studies because of the paucity of data during 136
 ice-covered seasons. In an attempt to circumvent this short- 137
 coming, Cooper et al. [2008] introduced the use of flow- 138
 weighted values of tracer concentrations, such as Ba in Arctic 139
 rivers. 140

[6] In the present work, we move beyond previous studies 141
 by documenting the spatial and temporal variability of dis- 142
 solved Ba in waters of the Canadian Arctic Archipelago 143
 over a complete annual cycle, as well as the relationship 144
 between Ba and measurable parameters of the inorganic 145
 carbon system, specifically the dissolved inorganic carbon 146
 (DIC) and A_T . We use results of a multitracer water mass 147
 analysis to assess the temporal evolution of freshwater 148
 addition and removal to/from the surface waters over the 149
 annual cycle, and compute the surface layer dissolved Ba 150
 deficiency - the difference between observed and “ideal” or 151
 conservative Ba concentrations - as a measure of bio-Ba 152
 formation. From this deficiency, we estimate the annual 153
 export of organic carbon (C_{org}) out of the euphotic zone and 154
 discuss the role of export and decay of bio-Ba below the 155
 surface layer in relation to the saturation state of waters with 156
 respect to barite. 157

2. Methods 158

2.1. Investigation Area 159

[7] This study was conducted in the framework of the 160
 International Polar Year on board the Canadian icebreaker 161
 CCGS Amundsen between September 2007 and September 162
 2008. Sampling in the Canadian Arctic Archipelago (CAA) 163
 took place at the beginning and end of the 12-month cruise 164
 at stations along an east-west section from Baffin Bay into 165
 the Eastern Beaufort Sea (Figure 1). The Amundsen Gulf, in 166
 the eastern Beaufort Sea (Figure 1), was sampled through 167
 a full annual cycle, for the very first time, at approximately 168
 bi-weekly intervals, at somewhat higher frequency during 169
 spring and summer than during winter, when, by design, the 170
 ship was frozen into free-drifting floes for varying periods 171
 of time. For the subsequent annual analysis, we constructed 172

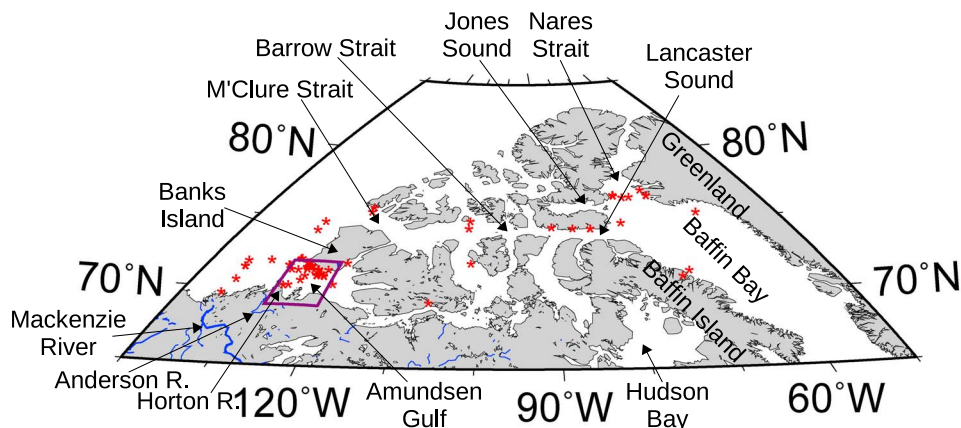


Figure 1. Investigation area. The stations sampled for dissolved Ba are indicated by red stars. The box encompasses the area 70°N–72°N, 121.8°W–126°W. The annual cycles and budgets reported in this paper were constructed from data collected at stations within this area. Hydrographic and carbonate system parameters are from higher temporal and spatial sampling densities [see *Shadwick et al.*, 2011b].

173 an annual cycle of observational data acquired in an area
174 defined by the boundaries: 70°N–72°N, 121.8°W–126°W
175 (Figure 1). Obviously, any considerations of interannual
176 variability would exceed the limitations of our data set.

177 2.2. Analytical Methods

178 [8] As part of the overall sampling program in the
179 Amundsen Gulf [e.g., *Shadwick et al.*, 2011b], we collected
180 seawater samples using a rosette system equipped with
181 24 12-L Niskin bottles at approximately 70 stations (includ-
182 ing repeats at different times of the year). Vertical profiles
183 of dissolved Ba concentrations were constructed from 8 to
184 12 depths per cast. Unfiltered seawater was transferred directly
185 from the spigot of the Niskin bottles into 30 mL plastic bottles,
186 acidified with 15 μL of concentrated Suprapur hydrochloric
187 acid and analyzed in the home laboratory using Isotope
188 Dilution Sector Field Inductively Coupled Plasma Mass
189 Spectrometry (SF-ICP-MS, Element 2, Thermo Finnigan).
190 Briefly, 1 g of seawater was spiked with 0.7 g of a ^{135}Ba -spike
191 solution yielding a $^{138}\text{Ba}/^{135}\text{Ba}$ ratio between 0.7 and 1 to
192 minimize error propagation. Subsequently the sample was
193 diluted with Milli-Q grade water to a final weight of 30 g.
194 Blanks consisted of acidified (with nitric acid) Milli-Q water.
195 Quantities of sample, spike and dilution water were accu-
196 rately assessed by weighing. Reproducibility of our method
197 is $\pm 1.5\%$ (RSD) as tested on repeat preparations of ref-
198 erence solutions. Average Ba values obtained for reference
199 waters SLRS-3 and an in-house standard (OMP, a Medi-
200 terranean Sea standard prepared by C. Jeandel) were $13.48 \pm$
201 $0.21 \mu\text{g l}^{-1}$ (1σ) with a RSD of 1.55% and $10.49 \pm 0.29 \mu\text{g}$
202 l^{-1} (1σ) with RSD of 2.75%, respectively, in good agreement
203 with certified values (SLRS-3: $13.4 \pm 0.6 \mu\text{g l}^{-1}$ and OMP:
204 $10.4 \pm 0.2 \mu\text{g l}^{-1}$). Overall precision (including sampling
205 precision) based on 6 dissolved Ba profiles sampled in a
206 hydrographically stable environment is $\pm 0.3 \mu\text{g l}^{-1}$ (1σ) with a
207 RSD of 5%. Please refer to *Dehairs et al.* [2008] and *Jacquet*
208 [2007] for further details. The Ba sampling was paralleled
209 by sampling for the stable isotope composition of seawater
210 ($\delta^{18}\text{O}$), of which samples were stored in 13 mL screw-
211 cap plastic test tubes without headspace. The $\delta^{18}\text{O}$ samples

were analyzed at the Geological Survey of Canada Delta- 212
Laboratory in Quebec City. Water samples were acidified 213
to pH ranging from 6 to 7 with orthophosphoric acid and 214
transferred without headspace to 4-mL vials containing 215
100 mg of copper to scavenge sulfide species and a few 216
grains of activated charcoal to scavenge organic volatiles. 217
After resting in the refrigerator for 5 days, 600 μL of water 218
were transferred to a 10-mL vial on a Gas Bench II and 219
equilibrated at 25°C for 5–7 days with a 0.5% CO_2 in 220
nitrogen gas mixture. The CO_2 gas was introduced and 221
analyzed in a Delta Plus mass ratio spectrometer. The oxygen 222
isotope ratio is expressed on the $\delta^{18}\text{O}$ notation, defined as the 223
 $^{18}\text{O}/^{16}\text{O}$ ratio of a sample relative to the Vienna Standard 224
Mean Ocean Water (V-SMOW) according to: 225

$$\delta^{18}\text{O} = \left(\frac{(^{18}\text{O}/^{16}\text{O})_{\text{sample}}}{(^{18}\text{O}/^{16}\text{O})_{\text{V-SMOW}}} - 1 \right) \times 10^3 [\text{‰}] \quad (1)$$

[9] The oxygen isotope composition of seawater was 226
measured to a precision of $\pm 0.05\text{‰}$, based on the analysis of 227
random duplicate samples. DIC and A_T were sampled 228
according to standard protocols [*Dickson et al.*, 2007] at 229
much higher spatial and temporal resolution, yielding more 230
than 2000 measurements. All samples were analyzed on 231
board by coulometric (DIC) and potentiometric (A_T) titration 232
using a VINDTA 3C (Versatile Instrument for the Deter- 233
mination of Titration Alkalinity, by Marianda, Germany). 234
Alternatively, A_T was also measured onboard using an 235
automated Radiometer® (Titralab 865) potentiometric titra- 236
tor operated in continuous titrant addition mode. Routine 237
calibrations and analyses of Certified Reference Materials 238
(provided by A. G. Dickson, Scripps Institution of Ocean- 239
ography) ensured that the uncertainty of the DIC and A_T 240
measurements was less than 0.5%. Details of the sampling 241
and analytical methods, as well as in-depth scientific eval- 242
uations of the DIC and A_T data, have been provided by 243
Shadwick et al. [2011a, 2011b] and *Mucci et al.* [2010]. 244

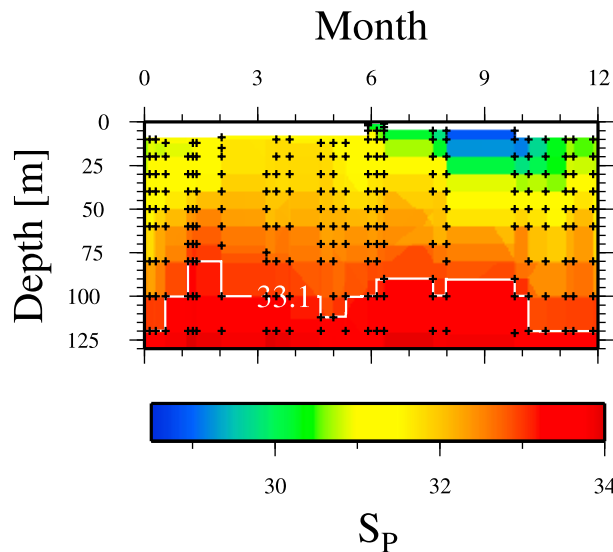


Figure 2. Temporal evolution of salinity in the surface waters of the Amundsen Gulf. Details of the seasonality of salinity and related carbon parameters have been discussed in detail by *Shadwick et al.* [2011b]. We have indicated the evolution of the $S_p = 33.1$ isopleth, which represents the lower boundary of our analysis.

245 2.3. Water Mass Decomposition

246 [10] As outlined in the following section, one of the
247 objectives of this study was to establish a surface layer
248 budget of dissolved Ba. Deviations from a conservative
249 behavior of dissolved Ba were estimated and attributed to
250 the formation of bio-Ba. Together with literature values for
251 the $C_{org}:bio\text{-Ba}$ ratio in particulate organic matter, we esti-
252 mate the export production out of the surface mixed layer
253 (SML). The maximum surface mixed layer depth in the
254 Amundsen Gulf is approximately 50 m, as determined from
255 the position of the pycnocline (Figure 2) [see also *Chierici*
256 *et al.*, 2011, Figure 2c; *Shadwick et al.*, 2011b]. We fur-
257 thermore assess the dissolved Ba surplus concentrations in
258 waters between 50 m depth and the level corresponding to
259 the practical salinity (S_p) = 33.1 isopleth, in order to eval-
260 uate whether decay of bio-Ba occurs within this depth
261 interval, just below the euphotic zone.

262 [11] In order to establish a dissolved Ba budget, we per-
263 formed a regional water mass analysis in the upper water
264 column, with the Upper Halocline Layer (UHL), charac-
265 terized by $S_p = 33.1$ (Figure 2), as the deepest layer. In
266 the Amundsen Gulf, the UHL water resides at a depth
267 of 80–120 m (Figure 2). Our analysis thus encompasses the
268 depth range of interest (0–50 m), as well as the layer
269 between 50 m and $S_p = 33.1$ isopleth, located at approxi-
270 mately 100 m water depth for most of the year.

271 [12] The application of salinity (S) and A_T to distinguish
272 the two major sources of freshwater, river runoff and sea-ice
273 melt, to seawater is well established [e.g., *Yamamoto-Kawai*
274 *and Tanaka*, 2005]. Here, we employ a three end-member
275 mixing model to decompose the water masses of the surface
276 layer in fractions of upper halocline water (F_{UHL}), meteoric
277 water (F_{MW} ; river runoff + precipitation), and sea-ice melt
278 (F_{SIM}). If the chemical properties of each end-member are

distinct and well defined, the relative contributions of these 279
three water masses to a parcel of seawater can be computed 280
from the following equations: 281

$$F_{MW} + F_{SIM} + F_{UHL} = 1 \quad (2)$$

$$F_{MW}S_{MW} + F_{SIM}S_{SIM} + F_{UHL}S_{UHL} = S \quad (3)$$

$$F_{MW}A_T(MW) + F_{SIM}A_T(SIM) + F_{UHL}A_T(UHL) = A_T \quad (4a)$$

$$F_{MW}\delta^{18}O(MW) + F_{SIM}\delta^{18}O(SIM) + F_{UHL}\delta^{18}O(UHL) = \delta^{18}O \quad (4b)$$

[13] The decomposition was performed using two sets of 282
equations: (2), (3), and (4a), as well as (2), (3), and (4b), 283
meaning that we used either A_T or $\delta^{18}O$ together with 284
salinity as tracers. In such analyses, as discussed for 285
example by B. Lansard et al. (Seasonal variability of water 286
mass distribution in the southeastern Beaufort Sea deter- 287
mined by total alkalinity and $\delta^{18}O$, submitted to *Journal of* 288
Geophysical Research, 2011), each tracer has its individual 289
strengths and weaknesses. For our purposes, relying on A_T 290
tends to more accurately describe the contributions of sea- 291
ice melt, at the expense of a slight underestimation of the 292
river runoff. On the other hand, the use of $\delta^{18}O$, better 293
describes the river runoff fraction, but tends to underesti- 294
mate the sea-ice fraction. Since we gathered much more 295
high quality A_T data than $\delta^{18}O$ data, we used salinity 296
together with A_T for the water mass decomposition analysis. 297
Consequently, our estimate of riverine Ba input should be 298
considered as a conservative, lower bound. 299

[14] The end-member characteristics are given in Table 1. 300
For the decomposition analysis, we assumed that S, A_T and 301
the Ba concentration in sea-ice are null, i.e., on an annual 302
cycle sea-ice does not constitute a net source or sink of these 303
species to the underlying seawater. Rather these species are 304
trapped during the ice formation in autumn and winter and 305
are released again during ice melt. Considering the sea-ice 306
concentrations of S, A_T , and Ba as being different from zero 307
at annual or greater time scales, leads to an erroneous def- 308
inition of ice as a source of these compounds, since the 309
corresponding extraction during ice formation is ignored. If 310
sea-ice concentrations are considered as different from zero, 311
the water mass decomposition analysis will yield much 312
larger meteoric fractions as a consequence [e.g., *Guay et al.*, 313
2009]. Furthermore, the effects of extraction and release of 314
the above compounds on our analysis is so small as to be 315
negligible for our purposes. The Ba concentrations in the 316
Horton River Estuary are similar to those reported for other 317
North American rivers [e.g., *Guay and Falkner*, 1998; 318
Cooper et al., 2008]. If we assume that there is only minor 319
seasonal variability in the riverine Ba concentrations [*Guay* 320
and Falkner, 1998], the Horton River Ba concentration 321
(295 nM Ba, Table 1) is close to the flow-weighted average 322
concentrations of the nearby Mackenzie (371 nM Ba) or 323
Yukon (369 nM Ba) Rivers [*Cooper et al.*, 2008]. 324

[15] Using the fractions of the individual components 325
 F_{SW} , F_{SIM} and F_{UHL} , we computed the “ideal” Ba con- 326
centrations (Ba_{ideal}) in the upper water column down to $S_p =$ 327
33.1, as outlined above. 328

$$F_{MW}Ba(MW) + F_{SIM}Ba(SIM) + F_{UHL}Ba(UHL) = Ba_{ideal} \quad (5)$$

t1.1 **Table 1.** End-Members and Characteristics Used for the Water
t1.2 Mass Decomposition Analysis^a

	A_T ($\mu\text{mol kg}^{-1}$)	Salinity (S_p)	Ba (nM)	$\delta^{18}\text{O}$ (‰)
t1.3 Meteoric water	1880.0	0	295	-20
t1.4 Sea-ice melt	0	0	0	-2.0
t1.5 Upper Halocline water	2283.0	33.1	69	-1.5

t1.6 ^aAll data were measured during our cruises. The meteoric water
t1.7 concentrations were measured in the Horton River Estuary during our
t1.8 program in spring 2008. $\delta^{18}\text{O}$ for sea-ice melt is adapted from *Bates*
t1.9 *et al.* [2009]. Salinity and A_T were used in the decomposition analysis,
t1.10 whereas Ba was used to compute the “ideal” Ba concentrations. Note that
t1.11 values quoted below may differ from those used in other studies [*Chierici*
t1.12 *et al.*, 2011] in the same area because of spatial and temporal variability.
t1.13 Furthermore, the null salinity and alkalinity ascribed to the sea-ice melt-
t1.14 water reflect the integrated annual effect of the ice cycle.

329 [16] Ba_{ideal} represents the expected Ba concentration if Ba
330 was a conservative property. For each sample, the difference
331 between the actual, i.e., observed Ba concentration (Ba_{obs}),
332 and Ba_{ideal} is used to compute the Ba deficiency, which we
333 attributed to Ba export (Ba_{exp}) from the surface layer due
334 to sinking of bio-Ba. In the discussion that follows we
335 adopt a ratio of $C_{\text{org}}:\text{bio-Ba} = 225 \text{ g C (g Ba)}^{-1}$ [2575 mol C
336 (mol Ba)⁻¹], an approximate average of the values reported
337 by *Dymond et al.* [1992], *Broecker and Peng* [1982], and
338 *Francois et al.* [1995]. The estimate by *Broecker and Peng*
339 [1982], ($C_{\text{org}}:\text{bio-Ba} = 260 \text{ g C (g Ba)}^{-1}$), served as an
340 upper bound, whereas values of $C_{\text{org}}:\text{bio-Ba} = 185\text{--}200 \text{ g C}$
341 (g Ba)^{-1} compiled by *Dymond et al.* [1992] are at the lower
342 limit, with the value of $C_{\text{org}}:\text{bio-Ba} = 215 \text{ g C (g Ba)}^{-1}$
343 reported by *Francois et al.* [1995] ranging in between. The

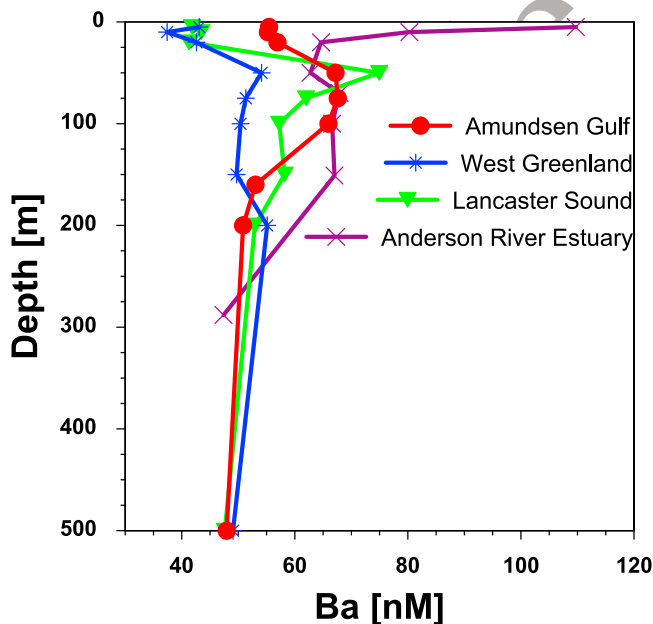


Figure 3. Dissolved Ba profiles from selected stations in the Canadian Arctic Archipelago and Baffin Bay. Individual dissolved Ba profiles are shown for four locations: the Mackenzie Shelf (purple line), the Amundsen Gulf (red line) and Lancaster Sound (green line), as well as near the west Greenland Coast (blue line). Please refer to insert for locations.

subsequent Ba inventory and carbon flux assessments were 344
computed for the upper 50 m of the water column. 345

3. Results and Discussion 346

3.1. Spatial Variability of Dissolved Ba Concentrations 347

[17] Profiles from selected stations across the CAA show 348
(Figure 3) the lowest Ba concentrations ($\sim 40 \text{ nM}$) in the 349
surface waters of eastern Baffin Bay and in the outflow of 350
Lancaster Sound into Baffin Bay. The Ba profile recorded in 351
the Amundsen Gulf (Figure 3) displays a nutrient-type 352
pattern with surface water concentrations of approximately 353
 $50\text{--}60 \text{ nM Ba}$. The high Ba concentrations ($65\text{--}70 \text{ nM Ba}$) 354
in the subsurface waters of the CAA (Figures 3 and 4) 355
correspond to an eastward flowing water mass [e.g., 356
Shadwick et al., 2011a] with a core salinity of 33.1, that is 357
characteristic of the Pacific or Upper Halocline water 358
mass. Irrespective of our sampling location, whether on the 359
eastern or western side of the CAA, Ba concentrations 360
converge to approximately 48 nM Ba in the deeper waters 361
of Atlantic origin. In the western-most profile, at a near- 362
shore station close to the Anderson River Estuary, Ba con- 363
centrations are elevated by runoff in the near surface layer 364
but also display nutrient-like characteristics in the subsur- 365
face waters. In the surface waters of the eastern part of the 366
CAA, the westward intrusion of water from Baffin Bay is 367

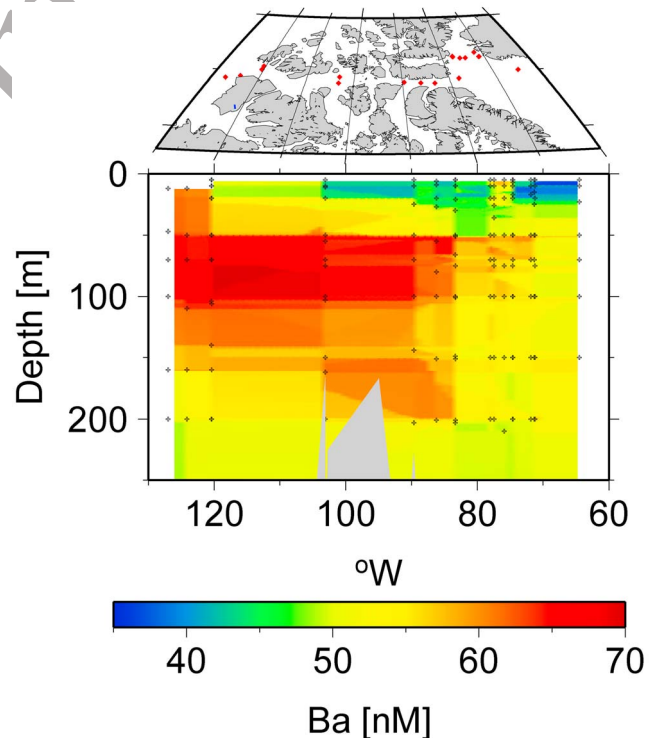


Figure 4. Distribution of dissolved barium in the Canadian Arctic Archipelago. We show the distribution of dissolved Ba along 75°N from the eastern Beaufort Sea to Baffin Bay and a subsequent cross section through Nares Strait. Please note the different Ba characteristics on the eastern (west of approximately 70°W , $[\text{Ba}] \approx 45 \text{ nM}$) and western (east of approximately 80°W , $[\text{Ba}] \approx 55 \text{ nM}$) sides of Nares Strait.

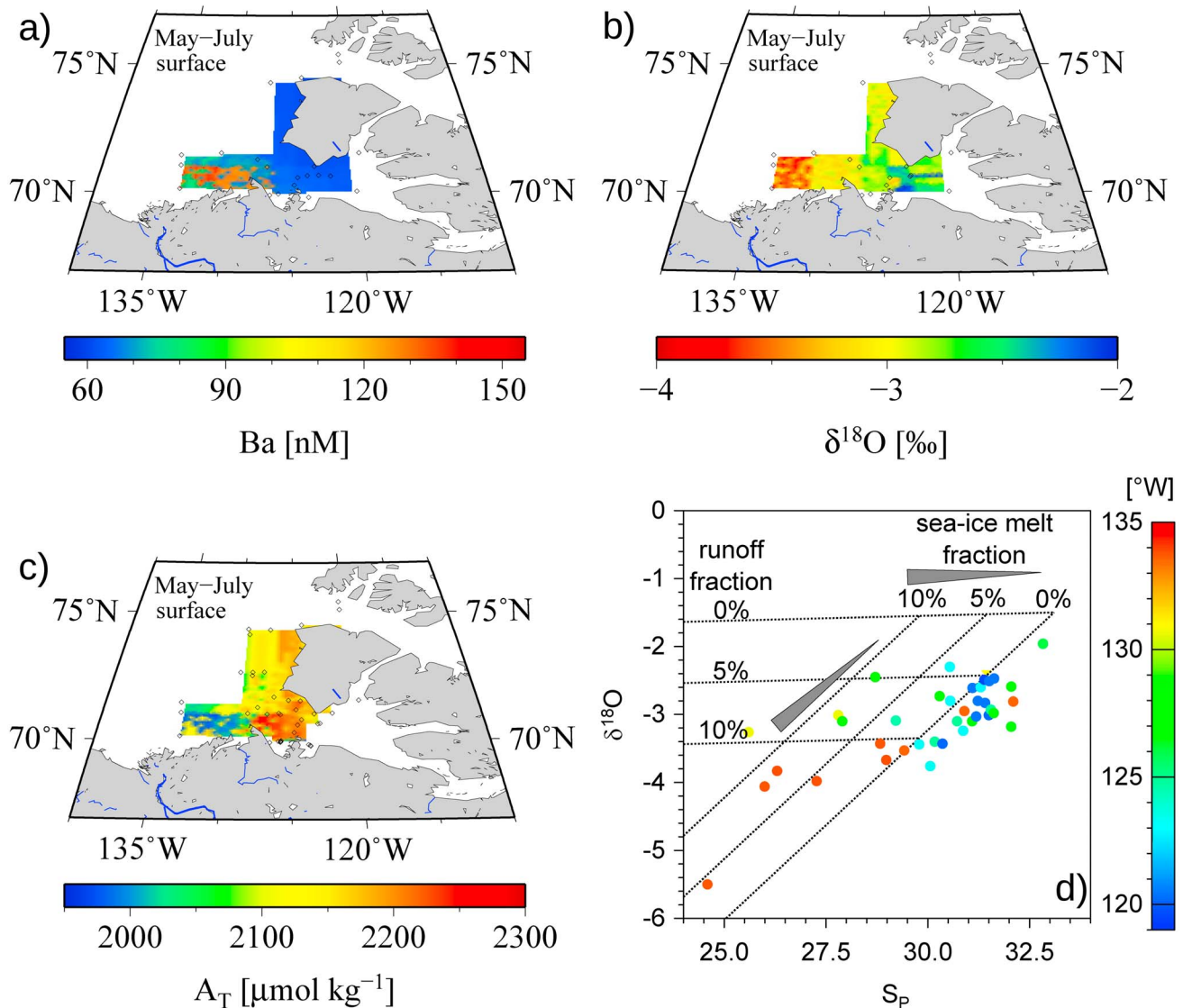


Figure 5. Distribution of Ba, $\delta^{18}\text{O}$, and A_T during Spring 2008. (a) Dissolved Ba, (b) $\delta^{18}\text{O}$, and (c) A_T in surface waters are shown as average observations made during the months of May, June, and July 2008. The elevated Ba and lower A_T concentrations near the mouth of the Anderson River correspond to more negative $\delta^{18}\text{O}$ values [e.g., Bates *et al.*, 2009]. (d) Following Macdonald *et al.* [1989] and Bates *et al.* [2009], freshwater from river runoff and sea-ice melt are distinguished on the basis of their salinity and $\delta^{18}\text{O}$ characteristics. The color coding in Figure 5d indicates the longitude of the sampling location.

368 evident from the low Ba concentrations (Figure 4). It is also
 369 interesting to note the presence of the northward flowing
 370 West Greenland Current [e.g., Münchow and Melling,
 371 2008], waters of Atlantic origin, characterized by low dis-
 372 solved Ba concentrations, on the eastern side of Nares Strait
 373 (Figure 4). The southward flowing waters on the western
 374 side of Nares Strait originate from the Arctic and are char-
 375 acterized by relatively high Ba concentrations, since the
 376 Arctic Ocean serves as collector for Arctic river water with
 377 elevated Ba concentrations [e.g., Guay and Falkner, 1998;
 378 Cooper *et al.*, 2008].

379 [18] After the ice breakup in late April and early May,
 380 river runoff affects the surface waters, in particular in the

western part of the study area (Figure 5). The surface
 381 salinity minimum caused by both river runoff and sea-ice
 382 melt is usually observed in September, corresponding to the
 383 minimum sea-ice coverage [e.g., Shadwick *et al.*, 2011b].
 384 In spring, i.e., during the months of May through July, we
 385 observed high dissolved Ba concentrations in nearshore
 386 areas, increasing in the westerly direction (Figure 5a) caused
 387 by the arrival of riverine freshwater with high Ba con-
 388 centrations. The early arrival of freshwater from rivers
 389 (compared to sea-ice melt) is also evident from the distri-
 390 bution of $\delta^{18}\text{O}$ in the mixed layer. Sea-ice $\delta^{18}\text{O}$ -values are
 391 approximately -2‰ [Bates *et al.*, 2009], therefore the sig-
 392 nificantly more negative values recorded in the surface
 393

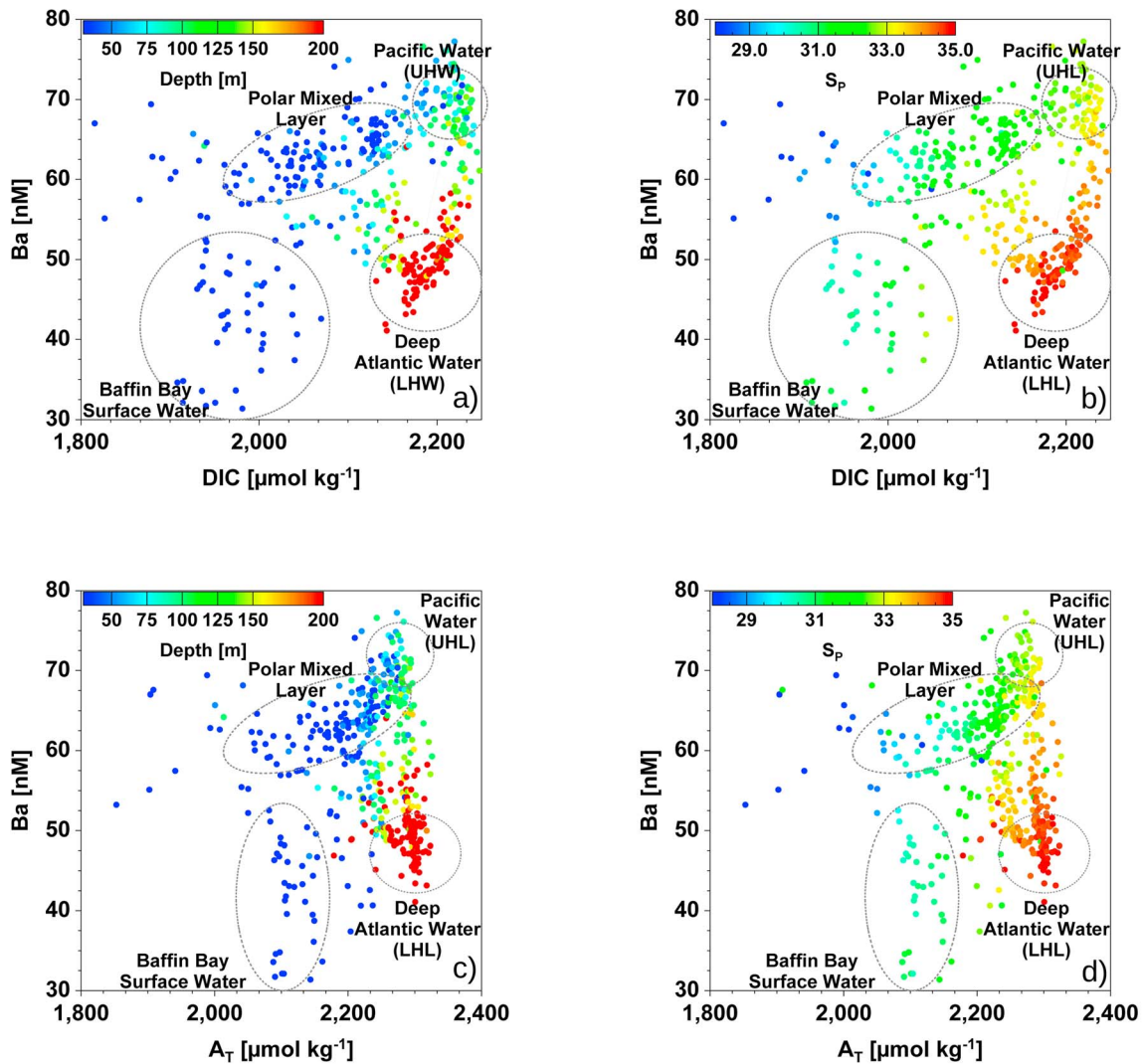


Figure 6. Relationship between carbonate system parameters and Ba. (a, b) Ba versus DIC and (c, d) Ba versus A_T are shown with corresponding depth (Figures 6a and 6c) or salinity (Figures 6b and 6d) values in color. The color coding does not reveal the full ranges of depth or salinity, but focuses on the 30–200 m depth range, where the gradients are strongest. Higher or lower values of salinity and depth are included within the maximum/minimum color, respectively. The lines are drawn to underline the conservative behavior of Ba and A_T in the deeper waters, in contrast to DIC, which clearly reveals the addition of metabolic CO_2 as shown by *Shadwick et al.* [2011a, 2011b]. The Pacific and deep Atlantic water masses are also called Upper and Lower Halocline Waters (UHL, LHL), respectively.

394 mixed layer in the western part of our study area ($\sim 4\%$)
 395 reflect inputs from runoff with a $\delta^{18}\text{O}$ signature of approx-
 396 imately -20% [Macdonald *et al.*, 1989; Cooper *et al.*, 2008;
 397 Bates *et al.*, 2009; Yi *et al.*, 2010] (Figure 5b). As a con-
 398 sequence of the arrival of riverine freshwater, A_T decreases
 399 in the western areas (Figure 5c), since riverine A_T con-
 400 centrations are lower than A_T concentrations of the
 401 Amundsen Gulf [e.g., *Shadwick et al.*, 2011a]. At this time
 402 of the year (May–July), our observed $\delta^{18}\text{O}$ composition of
 403 the surface waters, which is in good agreement with the
 404 above mentioned literature values, reveals little or no con-
 405 tribution by fresh water from sea-ice melt, whereas the
 406 runoff fraction clearly increases in the westerly direction
 407 (Figure 5d). The spatial distribution of the $\delta^{18}\text{O}$ composi-
 408 tion in surface waters shows a clear east to west gradient

(Figure 5b) with values at -2% in the Amundsen Gulf indi- 409
 410 cating a low influence of river runoff here, and more negative
 411 values of -4% in the western part close to the estuaries. This
 412 agrees with findings by *Magen et al.* [2010], *Shadwick et al.*
 413 [2011a], and *Cheirici et al.* (submitted manuscript, 2011), that
 414 little or no runoff from the Mackenzie or Horton rivers
 415 reaches the Amundsen Gulf at any time of the year.

[19] The relationship between dissolved Ba and DIC 416
 417 exposes two distinctly different regimes: the waters above
 418 and below the UHL (Figures 6a and 6b). Within the Polar
 419 Mixed Layer (PML), a mixture of SIM, MW and UHL, 419
 420 covering approximately the upper 50 m of the water column
 421 and with a S_p range between 29.5 and 31, the concentra-
 422 tions of Ba and DIC are positively correlated and increase
 423 with depth until they reach values similar to those in the

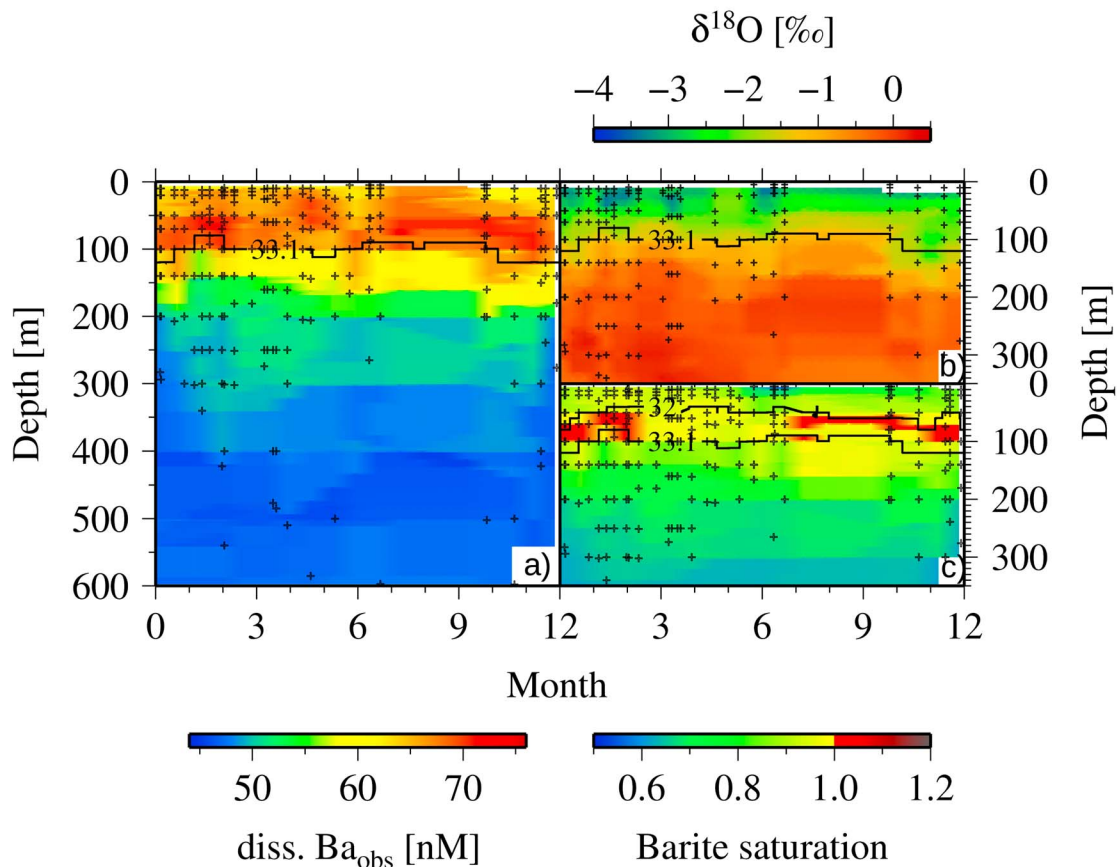


Figure 7. Temporal evolution of Ba, $\delta^{18}\text{O}$, and the barite saturation state in the Amundsen Gulf. (a) The dissolved Ba concentrations for the water column of the Amundsen Gulf. (b and c) We show $\delta^{18}\text{O}$ and the barite saturation state. We indicate the $S_p = 33.1$ isopleth, as well as the $S_p = 32$ isoline in Figure 7c, both encompassing approximately the depth range of 50 m to 100 m.

424 subsurface waters (50–100 m). Dissolved Ba concentrations
 425 are highest just above the UHL, originating from the Pacific
 426 at $S_p = 33.1$ (see also discussion in section 3.2.), while DIC
 427 continues to increase below the UHL due to the respiration
 428 of settling organic matter. Finally, both DIC and Ba con-
 429 centrations decrease in deeper waters (Figure 6a) as Atlantic
 430 Ocean Water is encountered. The A_T/Ba relationships
 431 (Figures 6c and 6d) exhibit similar patterns to the DIC/Ba
 432 relationships, but given the more conservative behavior of
 433 A_T , relative to DIC, stronger linear correlations are observed
 434 in the sub-halocline waters. The addition of metabolic
 435 DIC occurs at timescales that are shorter or similar to the
 436 residence time of the subsurface waters in the Amundsen
 437 Gulf (1–2 years [Lanos, 2009]; see also below section 3.4.),
 438 while the release of A_T and the dissolution or formation
 439 of barite occurs over longer, multiyear time scales, such that
 440 the A_T/Ba relationship appears to be dominated by water
 441 mass mixing (Figure 6d).

442 [20] We computed the Ba outflow from the Canadian
 443 Archipelago via Lancaster Sound in order to compare our
 444 observations with those of Taylor *et al.* [2003]. According
 445 to Ingram [2002; see also Shadwick *et al.*, 2011a], the
 446 outflow from Lancaster Sound into Baffin Bay is on the
 447 order of $1.1 \cdot 10^6 \text{ m}^3 \text{ s}^{-1}$. Using this estimate, a depth-

448 weighted water column average Ba concentration of 51.2 nM
 449 Ba (Figure 3), and a water column depth of 500 m, yields
 450 an annual dissolved Ba export from the CAA into Baffin Bay
 451 on the order of $1.6 \cdot 10^9 \text{ mol Ba yr}^{-1}$ or $222 \cdot 10^9 \text{ g Ba yr}^{-1}$
 452 ($56.3 \text{ mol Ba s}^{-1} / 7.7 \cdot 10^3 \text{ g Ba s}^{-1}$, respectively). Taylor *et al.*
 453 [2003] reported an outflow from the Canadian Archipelago
 454 of $89.7 \pm 7.6 \text{ mol Ba s}^{-1}$. Our estimate is smaller but of the
 455 same order of magnitude. Taylor *et al.* [2003] also considered
 456 the outflows from Jones Sound, Smith Sound, and Barrow
 457 Strait, whereas our estimate is restricted to the contribution
 458 from Lancaster Sound. Furthermore, it is worth noting that
 459 our depth-weighted average Ba concentration for Lancaster
 460 Sound (51.2 nM Ba) is slightly lower than the value reported
 461 by Taylor *et al.* [2003] ($62.4 \pm 5.1 \text{ nM Ba}$).

3.2. Dissolved Ba and Barite Solubility in the Amundsen Gulf

462
 463
 464 [21] We now investigate the temporal evolution of dis-
 465 solved Ba concentrations and of the saturation state of the
 466 waters with respect to barite (BaSO_4) in the Amundsen Gulf
 467 (Figures 7–9). The barite saturation state is expressed as:

$$\text{Saturation state} = \frac{Q_{(\text{BaSO}_4, \text{aq})}}{K_{S_p(\text{Barite})}} \quad (6)$$

468 where $Q_{(\text{BaSO}_4, \text{aq})}$ is the ion activity product of aqueous
 469 barium sulphate and $K_{\text{sp}(\text{Barite})}$ is the thermodynamic solu-
 470 bility product of barite [Monnin, 1999]. The $\text{BaSO}_4(\text{aq})$ ion
 471 activity product can be expressed as

$$Q_{(\text{BaSO}_4, \text{aq})} = m_{\text{Ba}^{2+}(\text{t}, \text{aq})} \cdot m_{\text{SO}_4^{2-}(\text{t}, \text{aq})} \cdot \gamma_{\text{BaSO}_4(\text{t}, \text{aq})}^2 \quad (7)$$

472 where m is the total molality of the designated aqueous
 473 species and γ is the total (or stoichiometric) mean activity
 474 coefficient of aqueous barium sulphate in seawater. The
 475 various thermodynamic quantities are calculated after
 476 Monnin [1999]. This model has been used to investigate the
 477 saturation state of the global ocean from the GEOSECS data
 478 [Monnin *et al.*, 1999]. A full description of the calculation
 479 of the barite saturation state from the measured quantities
 480 (dissolved Ba concentration, temperature, S_p and depth) is
 481 given by Hoppema *et al.* [2010].

482 [22] As indicated in Figure 3, dissolved Ba surface water
 483 concentrations are approximately 65.2 ± 2.4 nM Ba in the
 484 upper 50 m of the Amundsen Gulf, and nearly invariant
 485 throughout the year, except for a slight decrease during
 486 the later part of the year (Figure 7a). Within the subsur-
 487 face layer, bounded by the SML and the $S_p = 33.1$ isopleth,
 488 the dissolved Ba concentrations reach maximum values
 489 of approximately 68.5 ± 2.0 nM Ba. Here, as well, the

concentrations appear to be relatively constant throughout 490
 the year (Figure 7a). Below the UHL, the influence of deeper 491
 waters of Atlantic origin is reflected by decreasing Ba 492
 concentrations with depth to minimum values of approximately 493
 45 nM Ba (Figure 7a, 48.1 ± 1.9 nM Ba below 200 m; $47.4 \pm$ 494
 0.9 nM Ba below 300 m). The stable oxygen isotope 495
 composition of water (Figure 7b) reveals lowest values of 496
 approximately $\delta^{18}\text{O} = -3.6\text{‰}$ in the surface layer ($-2.7 \pm$ 497
 0.4‰ average in the upper 50m), and more positive values 498
 with depth to approximately $\delta^{18}\text{O} = -1.5\text{‰}$ in the UHL layer 499
 at $S_p = 33.1$ ($-1.7 \pm 0.4\text{‰}$ average between 50m and 100m), 500
 and most positive values of $\delta^{18}\text{O} = 0.76\text{‰}$ in the deep 501
 Atlantic layer ($0.0 \pm 0.3\text{‰}$ average below 200m, $0.0 \pm 0.3\text{‰}$ 502
 average below 300m, $0.3 \pm 0.3\text{‰}$ average below 500m). 503

[23] In order to distinguish between the two major pro- 504
 cesses, that shape the nutrient-type barium profile: (1) the 505
 release of Ba from decaying organic matter in the layer just 506
 below the euphotic zone, and (2) the mixing of the surface 507
 and subsurface water masses, we consider the saturation 508
 state of the waters with respect to barite (Figure 7c). The 509
 surface waters, i.e., the upper 50 m of the water column, are 510
 undersaturated with respect to barite throughout the year, 511
 particularly in June, which coincides with the maximum in 512
 net community production (NCP) [Shadwick *et al.*, 2011b] 513
 (see also discussion in section 3.3); yet closer to saturation 514
 during ice-covered winter months than during the ice-free 515
 season. In the subsurface layer, between 50 m and 100 m 516
 depth, the saturation state values reach a maximum with 517
 barite saturation observed between June and February. This 518

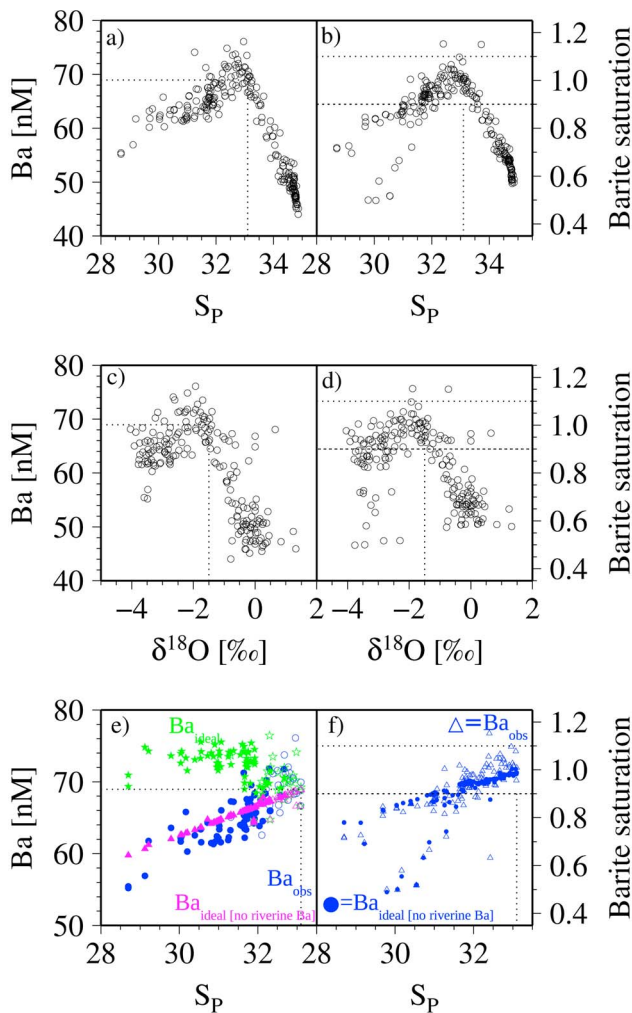


Figure 8. Property/property plots of Ba related and hydrographic parameters observed in the Amundsen Gulf. For the entire water column in the Amundsen Gulf, the relationships of dissolved Ba and the saturation state of barite (a, b) versus salinity and (c, d) versus $\delta^{18}\text{O}$ are shown. (e, f) Excerpts are shown for the upper part of the water column, i.e., for all samples with $S_p \leq 33.1$ (see Figure 2). Observed dissolved Ba concentrations (Ba_{obs}) are shown (blue dots), as well as the ideal Ba concentrations according to the three end-member mixing model (green diamonds). Furthermore, the model was run without riverine Ba ($\text{Ba}_{\text{ideal}\{\text{no Ba}_{\text{river}}\}}$, magenta triangles), which represents a conservative mixing between surface waters and UHL. The difference between Ba_{obs} and $\text{Ba}_{\text{ideal}\{\text{no Ba}_{\text{river}}\}}$ (Ba deficiency) is attributed to Ba export (Ba_{exp}) via sinking of organic matter (i.e., as bio-Ba). The conservative behavior of $\text{Ba}_{\text{ideal}\{\text{no Ba}_{\text{river}}\}}$ clearly emphasizes the importance of riverine Ba contributions to the surface layer Ba concentrations. Samples deeper than 50 m are plotted as open symbols, while shallower samples are plotted as solid symbols (Figure 8e). For samples with $S_p \leq 33.1$ we compare the observed barite saturation state (open symbols) with the barite saturation state computed with $\text{Ba}_{\text{ideal}\{\text{no Ba}_{\text{river}}\}}$. The Ba surplus at $S_p > 32$ is attributed to the decay of bio-Ba (Figure 8f). Please note that no river contribution can be detected below 50 m, approximately corresponding to $S_p > 32$ (see also Figure 7c). The dotted lines in all panels indicate the properties of the UHL waters (Table 1), and/or the equilibrium level of the barite saturation = 0.9–1.1, which inherently assumes an uncertainty of 10% in the computation of the barite saturation state [Monnin *et al.*, 1999].

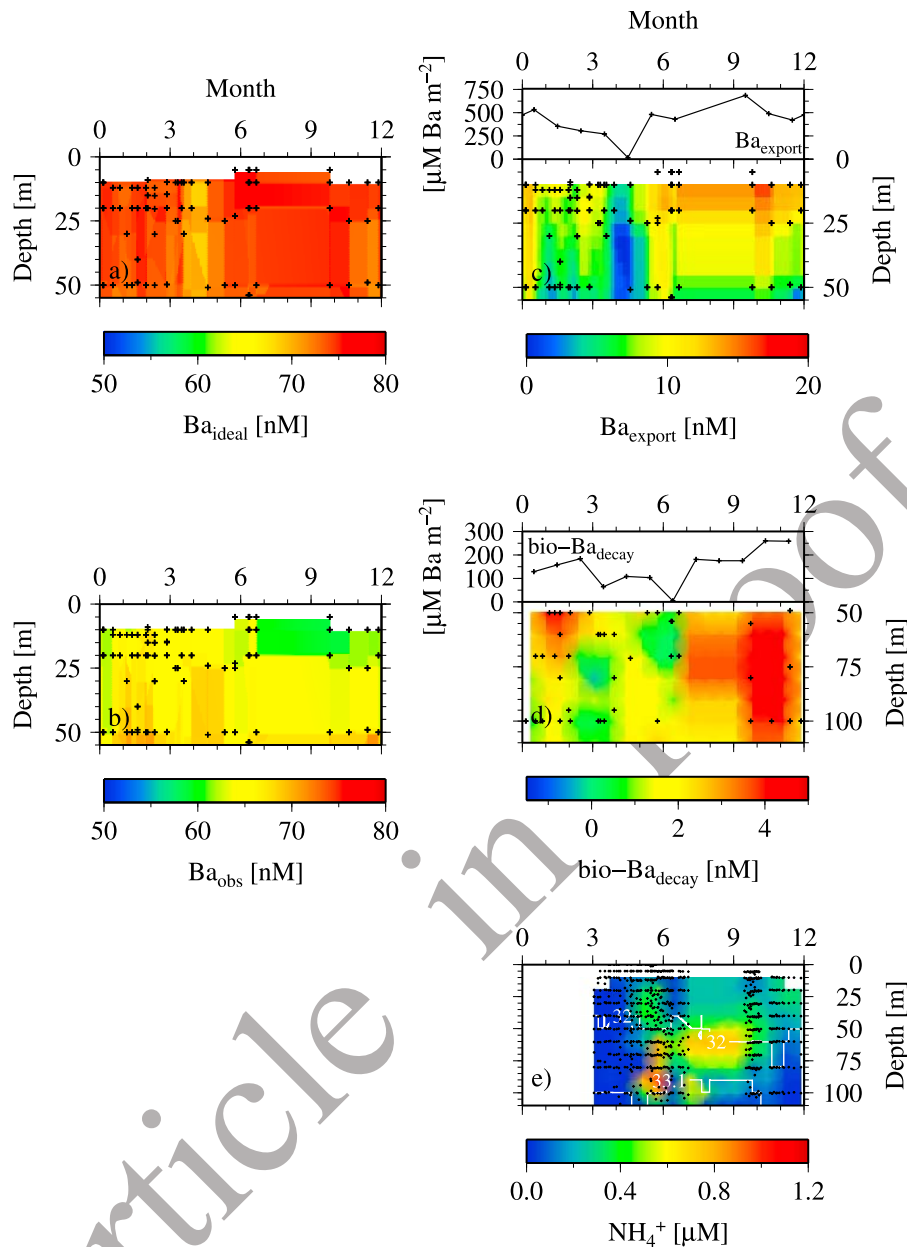


Figure 9. Time series of Ba_{ideal} , Ba_{obs} , Ba_{export} , decay of bio-Ba, and NH_4^+ for Amundsen Gulf. The seasonality of (a) Ba_{ideal} , (b) Ba_{obs} , and (c) Ba_{exp} for the upper 50 m of the water column in Amundsen Gulf is shown for a full annual cycle. Please note the change in the color scale in Figure 9c. We computed the decay of bio-Ba in the subsurface layer of the Amundsen Gulf as difference from the observations and the assumed conservative mixing between the surface layer and the UHL (lower panel, see also Figure 8f). The upper panel shows the integration of this Ba surplus over the depth range of 50 m to 100 m, i.e., approximately over the S_p range 32–33.1. For comparison, we show the seasonal evolution of NH_4^+ in the upper water column of Amundsen Gulf. NH_4^+ can be considered as a tracer of respiratory activity, thus indicating the arrival of sinking particulate organic matter and the onset of its respiration in the subsurface layer [see also *Forest et al.*, 2011].

519 layer is undersaturated with respect to barite only during the
 520 winter months before the onset of NCP in the surface layer.
 521 To summarize, the highest barite saturation states are found
 522 between the $S_p = 32$ isopleth at approximately 50 m water
 523 depth and the $S_p = 33.1$ isopleth corresponding to the UHL
 524 (Figure 7c), i.e., between the bottom of the surface mixed
 525 layer and the UHL. In the open ocean the bottom of the

surface mixed layer typically corresponds to the depth of
 526 maximum respiration rates [e.g., *Aristegui et al.*, 2005].
 527 The Amundsen Gulf is a shelf system and, clearly, is shall-
 528 lower than the open ocean, but nevertheless the maximum
 529 of respiratory activity, as indicated by the maximum of
 530 the ammonium concentrations (Figure 9e), and the highest
 531 barite saturation states coincide with the bottom of the
 532

533 surface layer. The occurrence of a barite saturation state
 534 maximum is best visualized in property/property plots of
 535 selected hydrographic parameters and dissolved Ba con-
 536 centrations or the barite saturation state (Figure 8). The dis-
 537 solved Ba versus salinity relationship highlights two distinct
 538 sections, each with nearly conservative behavior. A positive
 539 correlation of Ba and salinity is observed above the $S_p = 33.1$
 540 horizon. While the $S_p = 33.1$ layer is characterized by an
 541 average Ba concentration of 69 nM Ba (Table 1), the maxi-
 542 mum Ba concentration is actually found at lower salinities,
 543 thus above the $S_p = 33.1$ isopleth. Below the $S_p = 33.1$ iso-
 544 pleth, dissolved Ba concentrations decrease with increasing
 545 salinity reaching a minimum in the deep waters of Atlantic
 546 origin (Figure 8a). Similarly, the highest dissolved Ba values,
 547 and the only barite-equilibrated waters, are observed above
 548 the depths of the 33.1 isopleth (Figure 8b) between approx.
 549 50 m and 100 m depth (Figure 7c). Above and below this
 550 level the water column is undersaturated with respect to
 551 barite. The group of particularly low barite saturation states at
 552 salinities of 30–31 is associated with warm waters in July
 553 [see, e.g., *Shadwick et al.*, 2011b, Figure 6b]. Similar features
 554 arise when plotting dissolved Ba concentrations or the barite
 555 saturation state versus $\delta^{18}\text{O}$: the $\delta^{18}\text{O}$ signature of the $S_p =$
 556 33.1 isopleth is approximately $\delta^{18}\text{O} = -1.5\text{‰}$ (Table 1),
 557 while both the dissolved Ba concentrations and the barite
 558 saturation state maximum correspond to values of $\delta^{18}\text{O} \approx$
 559 -2‰ (Figure 8c and 8d). Using the results of the subsequent
 560 water mass decomposition analysis down to the S_p level of
 561 33.1 as a composite of MW, SIM, and UHL water (see
 562 equation (2)), we provide further evidence for the enrichment
 563 of dissolved Ba above the $S_p = 33.1$ layer. If we assume, as a
 564 thought experiment, that the meteoric Ba concentrations are
 565 zero (i.e., $\text{Ba}_{\text{ideal}\{\text{no Ba}_{\text{river}}\}}$) as detailed in the following
 566 section, the Ba versus salinity relationship becomes conser-
 567 vative and reflects a linear mixing of the PML and UHL
 568 waters (Figures 8e and 8f). If we compare these results with
 569 our measurements, we see that in the salinity range between
 570 $S_p = 32$ and $S_p = 33.1$ the observed Ba concentrations and
 571 the barite saturation state appear elevated relative to the
 572 conservative Ba (i.e., $\text{Ba}_{\text{ideal}\{\text{no Ba}_{\text{river}}\}}$) versus S relation-
 573 ship. In fact, the only values corresponding to barite satura-
 574 tion correspond to those that deviate from the linear Ba versus
 575 S relationship between the $S_p = 32$ and $S_p = 33.1$ (see open
 576 circles and triangles in Figures 8e and 8f). Since the contri-
 577 bution of MW to subsurface waters is negligible, we attribute
 578 the dissolved Ba surplus in the subsurface layer within the
 579 32 to 33.1 S_p range to the release of Ba from decaying
 580 organic matter (bio- Ba_{decay}), which sank out of the surface
 581 layer (Figures 9c and 9e). This Ba surplus peaks in late autumn,
 582 coinciding with the accumulation of dissolved organic carbon
 583 (DOC) and DIC in this subsurface layer in response to organic
 584 matter decay [see *Shadwick et al.*, 2011b, Figures 8c and 8d].
 585 Integrating this Ba surplus over the 50–100 m depth range
 586 yields a maximum Ba release of approximately 260 μM Ba
 587 m^{-2} (Figure 9c), corresponding to approximately 40% of the
 588 bio-Ba formed in the surface layer (Figure 10). The degrada-
 589 tion of settling organic matter and the concomitant release
 590 of Ba to the water column explains the nutrient-like behavior
 591 of dissolved Ba. A further, biologically mediated process
 592 affecting dissolved Ba concentrations is the precipitation of
 593 barite, which is associated with enhanced respiratory activity
 594 [e.g., *Dehairs et al.*, 1992]. This process, however, cannot be

detected in our dissolved Ba measurements, since the amount
 of barite precipitation is approximately three orders of mag-
 nitude lower than the bio-Ba turnover.

3.3. Variability of Ba in the Amundsen Gulf and Export of Ba out of the Surface Layer

[24] In order to arrive at an annual budget for dissolved Ba
 for the Amundsen Gulf area (Figure 1), we employ a three
 end-member mixing model for the upper water column. The
 three end-members are meteoric water, sea-ice meltwater
 and Upper Halocline Water, as defined by their respective
 A_T , salinity and $\delta^{18}\text{O}$ values (Table 1). The model yields the
 temporal evolution of their respective fractions over the
 course of the year. The maximum SIM contribution was
 10% in October, whereas MW reached a maximum at 5% in
 the spring. Compared to the analysis of *Guay et al.* [2009],
 our values are higher for SIM and lower for MW, respec-
 tively. This discrepancy may reflect both a seasonal bias, as
Guay et al. [2009] sampled only in summer during the
 salinity minimum, and the assumption that sea-ice con-
 stitutes a net annual source of salt. As noted previously this
 assumption is only valid at a seasonal time scale and at an
 appropriate spatial scale.

[25] On the basis of the above mixing analysis, we com-
 puted “ideal” Ba concentrations (Ba_{ideal}) (equation (5))
 under the assumption that dissolved Ba behaves conserva-
 tively. In order to highlight the role of riverine dissolved Ba,
 we also show the observed Ba (Ba_{obs}), together with Ba_{ideal}
 and $\text{Ba}_{\text{ideal}\{\text{no Ba}_{\text{river}}\}}$, the latter computed under the
 assumption that the MW does not carry any dissolved Ba
 (Figures 8e and 8f). The $\text{Ba}_{\text{ideal}\{\text{no Ba}_{\text{river}}\}}$ displays a near
 perfect conservative relationship to salinity, but it clearly
 underestimates Ba_{obs} . The riverine Ba contributed up to 15%
 of the Ba inventory in the upper 50 m of the water column
 (Figure 10a). We attribute the deficiency between Ba_{obs}
 and Ba_{ideal} to Ba export (mainly as bio-Ba) out of the sur-
 face layer (Ba_{exp} , Figure 8e) and computed Ba_{exp} for each
 observation throughout the annual cycle (Figures 9 and 10).
 The Ba deficiency in the surface layer and thus Ba_{exp} peaked
 in late summer/early autumn, when biological activity waned.
 The Ba_{exp} was lowest during the salinity maximum in late
 winter, just before the onset of increased biological activity
 triggered by longer daylight hours and ice melt, and shortly
 before the delivery of significant amounts of riverine Ba. In
 the subsurface layer below 50 m, Ba_{ideal} and Ba_{obs} are more
 similar (i.e., $\text{Ba}_{\text{exp}} = 0$), indicating that the bio-Ba is primarily
 formed in, and exported from, the euphotic zone. The onset of
 the Ba export out of the surface layer (Figure 9c) is nicely
 mirrored by the rise of the ammonium (NH_4^+) concentrations
 [*Forest et al.*, 2011] in the subsurface layer (Figure 9e),
 interpreted as an indicator of the arrival of sinking organic
 matter and is subsequent respiration. The high turnover rates
 of NH_4^+ prevent its accumulation in the water column, in
 contrast to the build-up of the Ba deficiency in the surface
 layer throughout the seasons. Within the subsurface layer, the
 build-up of the bio- Ba_{decay} (Figure 9d) occurs somewhat
 delayed with respect to the onset of the Ba deficiency in
 the surface layer (Figure 9c) and the beginning of enhanced
 NH_4^+ concentrations in the subsurface layer (Figure 9e). On the
 other hand, as mentioned above, the rise of bio- Ba_{decay}
 appears concomitant to the increase of DOC concentrations
 in the subsurface layer [*Shadwick et al.*, 2011b, Figure 8d],

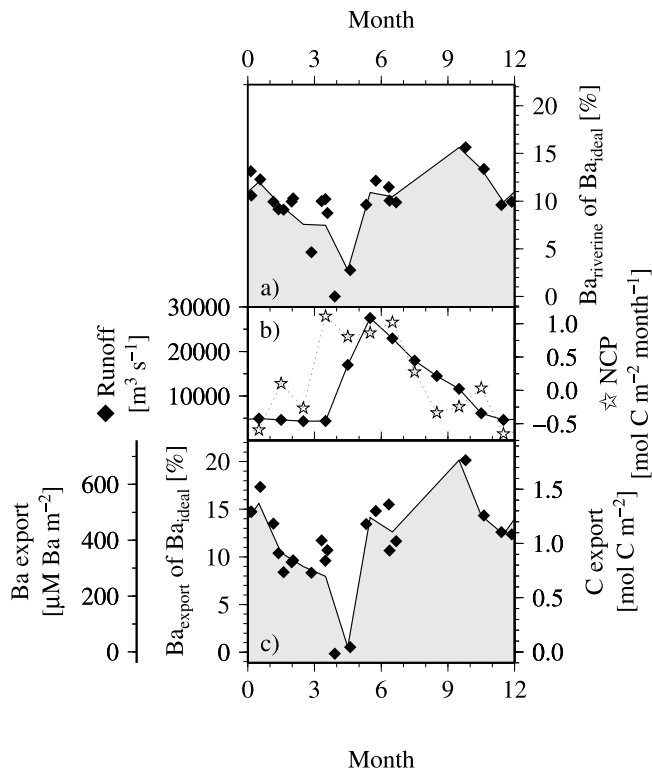


Figure 10. Temporal evolution of Ba-related inventories in the upper 50 m of the water column. (a) The fraction of riverine Ba, which is exported. (b) The temporal evolution of river runoff and NCP (NCP after *Shadwick et al.* [2011b] and river runoff after *Prange* [2002]; see also Water Survey of Canada, http://www.wsc.ec.gc.ca/staflo/index_e.cfm?cname=flow_daily.cfm). (c) Export of Ba and derived carbon export are shown as well as the fraction of Ba_{ideal} , which is exported. Squares indicate individual data, whereas shaded areas represent the monthly averages (Figures 10a and 10c). The lowest fraction of riverine Ba (Figure 10a) coincided with the salinity maximum, and the highest fraction with the salinity minimum. Increased Ba export (Figure 10c) coincided with the under-ice algal bloom, slightly earlier than the arrival of riverine freshwater (Figure 10b). Ba export exceeded the riverine Ba inputs. Ba and carbon exports peak in late summer, at the end of the biologically active period (Figure 10b).

656 as both originate from the decay of organic matter, and both
657 are more stable than NH_4^+ . The sinking rates of organic par-
658 ticles vary over a wide range, from a few meters to a few
659 hundred meters per day [e.g., *Kellogg et al.*, 2011; *Armstrong*
660 *et al.*, 2009]. Assuming slowly sinking particles with sink-
661 ing rates $<3 \text{ m d}^{-1}$, as reported for the investigation area
662 [*Kellogg et al.*, 2011], the settling time would be on the order
663 of 1–2 months. This would be in general agreement with the
664 findings discussed here, such as the delay between the rise
665 of Ba_{exp} and bio- Ba_{decay} in the surface and subsurface layers,
666 respectively (Figures 9c and 9d).

667 3.4. Export Production of Carbon

668 [26] We estimated the export of particulate organic carbon
669 from the surface layer by assuming that it is tightly related to

the bio-Ba flux [e.g., *Bishop*, 1988; *Dehairs et al.*, 1992, 670
1997; *Dymond et al.*, 1992; *Francois et al.*, 1995; *Dymond* 671
and Collier, 1996; *Gillikin et al.*, 2006; *Sternberg et al.*, 672
2007; *Calvert and Pederson*, 2007] and that the latter can 673
be computed from the dissolved Ba deficiencies in the upper 674
50 m of the water column (Figure 8e). We employed an 675
average ratio of $C_{org}:bio-Ba = 225 \text{ g C (g Ba)}^{-1}$ [2575 mol C 676
(mol Ba) $^{-1}$], adopted from *Dymond et al.* [1992], to estimate 677
the export of particulate organic carbon from the surface layer. 678
Our results indicate that the bio-Ba and organic carbon export 679
fluxes from the upper 50 m of the water column (Figure 10b) 680
were smallest toward the end of winter ($\sim 0.3 \text{ mol C m}^{-2}$), before 681
the onset of increased biological activity led by the proliferation 682
of ice and under ice algae, when ice cover still persisted [e.g., 683
Horner and Schrader, 1982; *Lavoie et al.*, 2009]. River runoff and 684
the associated supply of riverine Ba lag behind the increase in 685
 Ba_{exp} (Figure 10b), highlighting the contribution of ice 686
algae and under-ice algae to the initial spring export of 687
organic carbon out of the surface layer. The time lag 688
between the onset of export production and the increased 689
(under ice) carbon fixation, i.e., of net community produc- 690
tion (NCP) [see *Shadwick et al.*, 2011b], is consistent with 691
the seasonal evolution of biological activity in the Canadian 692
Arctic [*Horner and Schrader*, 1982; *Carmack et al.*, 2004; 693
Lavoie et al., 2009]. NCP remains high after the peak river 694
discharge, but wanes in late summer, when heterotrophic 695
processes begin to out-compete organic matter production. 696
Around September, the export of organic matter, i.e., Ba_{exp} , 697
reaches its maximum. From the perspective of the dissolved 698
Ba pool, the riverine Ba was efficiently captured by bio-Ba 699
formation, since the “new” Ba arrived just when biological 700
activity was highest (Figure 10b). This may explain the lack 701
of strong seasonality in dissolved (observed) Ba (Figure 9b) 702
profiles, as Ba_{exp} and $Ba_{riverine}$ displayed a similar season- 703
ality (Figures 10a, 10b, 9a, and 9c), but with opposing effects 704
on Ba_{obs} . Assuming that Ba_{exp} integrates the organic carbon 705
export at the annual scale, the Ba_{exp} maximum corresponds 706
to an annual organic carbon export of approximately 1.8 mol C 707
 $\text{m}^{-2} \text{ yr}^{-1}$. Since estimates of primary productivity span 708
over a rather wide range ($4.4 \pm 1 \text{ mol C m}^{-2} \text{ yr}^{-1}$, assuming 709
that this result, obtained by *Forest et al.* [2011] for the period 710
March–August, is representative for the entire year; $7\text{--}15 \text{ mol C}$ 711
 $\text{m}^{-2} \text{ yr}^{-1}$, based on satellite data [*Arrigo and van Dijken*, 712
2004]), and particle export studies cover only parts of the 713
annual cycle [*Forest et al.*, 2011; *Magen et al.*, 2010], 714
their relationship to our findings cannot readily be appre- 715
ciated. Nevertheless, our estimated carbon export (1.8 mol C 716
 $\text{m}^{-2} \text{ yr}^{-1}$) would represent 12–40% of the estimated primary 717
production [*Arrigo and van Dijken*, 2004; *Forest et al.*, 718
2011], which is in a reasonable range [e.g., *Buesseler*, 719
1998]. It should be noted that the primary production esti- 720
mate by *Arrigo and van Dijken* [2004] was derived from 721
satellite observations and does not account for under-ice 722
algal or subsurface production [e.g., *Tremblay et al.*, 2008; 723
Mundy et al., 2009]. *Shadwick et al.* [2011b] applied an 724
inorganic carbon budget technique to derive a NCP of 725
approximately $2.1 \text{ mol C m}^{-2} \text{ yr}^{-1}$ for the Amundsen Gulf 726
region, 40% of which is supplied by under-ice productivity. 727
According to our estimate, most of the NCP is exported out 728
of the surface layer. Two independent, but similar estimates 729
730

731 of the inventories of respired carbon dioxide (CO₂) in the
 732 subsurface waters (50–300 m) of the Amundsen Gulf were
 733 recently reported [Shadwick *et al.*, 2011a, 2011b]: 3.8 mol C
 734 m⁻² yr⁻¹ and 4.1 mol C m⁻². The former was derived by
 735 assuming an 18-month residence time for subsurface waters
 736 [Lanos, 2009], in line with previous estimates [Yamamoto-
 737 Kawai *et al.*, 2008; Hansell *et al.*, 2004] in the region. Our
 738 estimate of export production (1.8 mol C m⁻² yr⁻¹) and the
 739 respired CO₂ inventory of 4.1 mol C m⁻² derived by
 740 Shadwick *et al.* [2011a] yield a residence time of the sub-
 741 surface waters in the Amundsen Gulf on the order of two
 742 years, if all the exported carbon is respired in the subsurface
 743 waters, in agreement with the residence time reported by
 744 Lanos [2009].

745 [27] The timing of the carbon export reconstructed from
 746 this study (Figure 10b) is corroborated by Forest *et al.*
 747 [2008], who, based on sediment trap data, reported that
 748 the maximum POC contribution to the overall particle flux
 749 was observed in May and July, coinciding with the under-
 750 ice and pelagic algae blooms and their respective contribu-
 751 tions to NCP [Horner and Schrader, 1982; Shadwick *et al.*,
 752 2011b; see also Carmack *et al.*, 2004]. It should be noted,
 753 however, that the data of Forest *et al.* [2008] were collected
 754 in 2003/2004 and were acquired at a slightly different
 755 location. The latter may be of some importance since Forest
 756 *et al.* [2008] sampled west of our study area (Figures 1 and 5),
 757 likely under a stronger influence of the Mackenzie River
 758 plume. Our estimate of export production also depends on
 759 the choice of the C_{org}:bio-Ba flux ratio. The ratio we used
 760 in this study [C_{org}:bio-Ba = 225 g C (g Ba)⁻¹ or 2575 mol C
 761 (mol Ba)⁻¹] was derived from global or basin-wide estimates
 762 in various ocean basins. As noted by Dymond *et al.* [1992],
 763 their C_{org}:bio-Ba flux ratio (185–200 g C (g Ba)⁻¹) agrees to
 764 within 15% of the global estimate reported by Broecker and
 765 Peng [1982] (260 g C (g Ba)⁻¹). On the other hand, as argued
 766 by Dehairs *et al.* [2000] and Sternberg *et al.* [2007], the C_{org}:
 767 bio-Ba flux ratio may be higher along continental margins,
 768 but this has not yet been confirmed for the Arctic shelves.
 769 Irrespective of this, higher C_{org}:bio-Ba flux ratios have been
 770 attributed to higher carbon fluxes from coastal or margin
 771 sites, which in turn would allow our method to assess the
 772 export of marine carbon only. This would help constrain
 773 results of sediment trap studies, such as those of Forest *et al.*
 774 [2008, 2011] or Magen *et al.* [2010] by providing informa-
 775 tion about the source of the organic matter in the traps. A
 776 larger C_{org}:bio-Ba flux ratio would yield higher estimates of
 777 our carbon export and would exceed the NCP estimated by
 778 Shadwick *et al.* [2011b]. Furthermore, our estimate depends
 779 on the riverine Ba concentrations, such that an increase of
 780 the riverine Ba concentration by 33% (393 nM Ba instead of
 781 295 nM Ba, Table 1) would increase the carbon export
 782 estimate by 24%. Despite the overall uncertainties of our
 783 approach, our estimated carbon export of 1.8 mol C m⁻² yr⁻¹,
 784 derived from a complete annual data set, serves to better
 785 constrain carbon fluxes and production estimates. In addition,
 786 since bio-Ba formation and, thus, the Ba fluxes out of the
 787 surface layer are closely linked to biological processes in
 788 the marine water column, our approach can help unravel
 789 the sources of settling organic particles, may they be marine
 790 or terrestrial, inorganic or organic [e.g., Forest *et al.*, 2008;
 791 Magen *et al.*, 2010].

3.5. The Role of Export Production in the Carbon Budget of Amundsen Gulf

792
793

[28] In order to better understand the carbon dynamics of
 our study area, we establish a carbon budget over the annual
 cycle using our data and information available from the liter-
 ature. We considered processes (Figure 11) and assump-
 tions detailed in this section. We derived the CO₂ air-sea
 exchange from Shadwick *et al.* [2011b], assuming that sea-
 ice is impermeable to CO₂, but acknowledge that the latter is
 currently a focus of ongoing research [e.g., Semiletov *et al.*,
 2004; Zemmeling *et al.*, 2006; Papakyriakou and Miller,
 2011; Miller *et al.*, 2011; Else *et al.*, 2011; N.-X. Geilfus
et al., pCO₂ dynamics and related air-ice CO₂ fluxes in the
 Arctic coastal zone (Amundsen Gulf, Beaufort Sea, Canada),
 submitted to *Journal of Geophysical Research*, 2011]. We
 considered the diffusion of DIC from the subsurface layer
 into the surface layer (upper 50 m) according to Shadwick
et al. [2011b]. Since under-ice [Horner and Schrader, 1982;
 Juul-Pedersen *et al.*, 2010] and subsurface [Tremblay *et al.*,
 2008] production plays a crucial role in Arctic Ocean pro-
 ductivity but cannot be captured by satellite imagery, we rely
 on the primary production estimate by Forest *et al.* [2011],
 employing a food web model for the period of our observa-
 tions. We assume that this primary production estimate,
 obtained for the period March–August 2008, is representative
 of the overall annual production. We derived NCP from
 Shadwick *et al.* [2011b], who balanced the inorganic carbon
 budget in the water column of the Amundsen Gulf. Export
 production was assessed in this work and we assume that
 the export of particulate Ba mirrors the export of marine
 organic matter. Hence, given the export of marine carbon of
 0.45 mol C m⁻² yr⁻¹ (see below) out of the subsurface layer
 (50–100 m), 1.35 mol C m⁻² yr⁻¹ of the 1.8 mol C m⁻² yr⁻¹
 exported from the surface layer is respired in the subsurface
 layer. We considered two estimates for the respiration of
 organic matter in the subsurface water column: (a) derived
 from an inorganic carbon budget (3.8 mol C m⁻² yr⁻¹
 [Shadwick *et al.*, 2011b]), and (b) using an estimate of the
 water column inventory of respired DIC according to
 Shadwick *et al.* [2011a]. The latter approach was applied
 to our investigation area, yielding an inventory of 4.1 mol
 C m⁻². Given an 18-month residence time for water below
 the surface layer, as estimated from a set of hydrographic
 moorings in the Amundsen Gulf in 2003–2004 [Lanos,
 2009], this corresponds to an annual production of 2.7 mol
 C m⁻² yr⁻¹ for respiratory DIC. The particulate marine and
 terrestrial organic carbon flux out of the subsurface layer
 was estimated according to Forest *et al.* [2008, Figure 8b].
 This flux estimate, although from a slightly different area,
 covers almost a full year of observations, compared to that of
 Forest *et al.* [2011], which cover the period February to July.
 The extended temporal coverage by Forest *et al.* [2008] is
 of particular relevance, since our study, and Forest *et al.*
 [2008], reveal maximum C-export values during summer
 and autumn (Figure 10), a period not covered by Forest *et al.*
 [2011]. The benthic respiration was estimated from the par-
 ticle and sediment biogeochemical study of Renaud *et al.*
 [2007] using their average sediment oxygen demand of
 5 mmol O₂ m⁻² d⁻¹. When an O₂ consumption to metabolic
 CO₂ production ratio of 1.3 [Millero, 2006] is applied for
 either 6 or 12 months, benthic respiration yields a DIC release

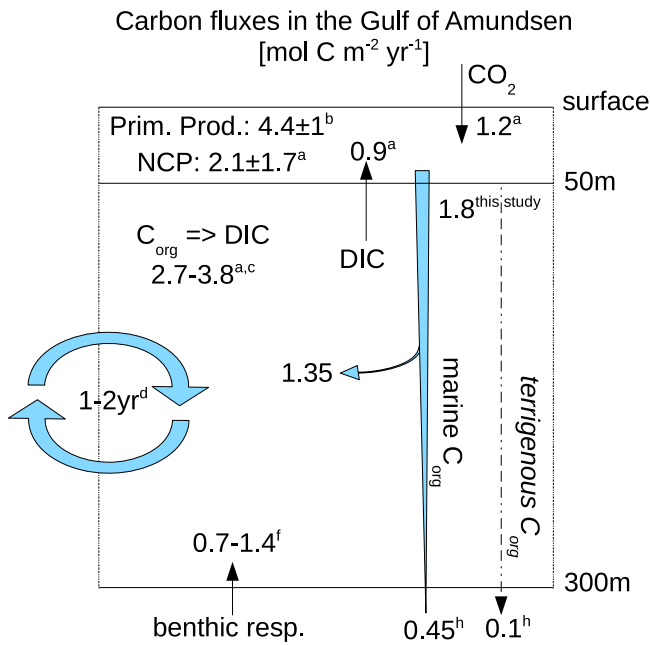


Figure 11. Carbon budget for Amundsen Gulf. Literature values and results of this work are used to estimate the carbon budget for the Amundsen Gulf. Since data were compiled from different years, the budget is climatological rather than for a specific year. Details of the individual terms are given in the text. Sources and times of observations denoted by superscript letters as follows: a, *Shadwick et al.* [2011b], 2007–2008; b, *Forest et al.* [2011], 2008; c, *Shadwick et al.* [2011a], 2007; d, *Lanos* [2009], 2002–2004; f, *Renaud et al.* [2007], 2004; h, *Forest et al.* [2008], 2003–2004.

853 from the surface sediments to the overlying water column
854 of $0.7\text{--}1.4\text{ mol C m}^{-2}\text{ yr}^{-1}$. We assume that there is no
855 net sediment accumulation, i.e., no net carbon burial occurs
856 over annual time-scales in the investigation area [*Richerol*
857 *et al.*, 2008].

858 [29] Despite the considerable uncertainties inherent to all
859 estimated fluxes, the budget presented here can be consid-
860 ered as balanced. The ratio between primary production and
861 NCP or export production [*Arrigo and van Dijken*, 2004;
862 *Forest et al.*, 2011; *Shadwick et al.*, 2011b], respectively, all
863 of which are derived from independent assessments, is on
864 the order of 0.15–0.4. The similarity between the NCP and
865 export fraction supports the hypothesis and observation that,
866 at the annual scale, organic matter does not accumulate in
867 the surface waters. The slightly elevated primary production
868 to export production ratio can be justified by the fact that the
869 under-ice production, which contributes approximately 50%
870 of NCP [*Shadwick et al.*, 2011b], is dominated by diatoms
871 with heavy frustules that sink rapidly [*Horner and Schrader*,
872 1982; *Juul-Pedersen et al.*, 2010]. Furthermore, the spring
873 open water bloom coincides with the peak in river runoff
874 (Figure 10b), which delivers a significant amount of ballast
875 material from land and, in turn, promotes the sinking of
876 marine organic matter, as observed in sediment trap studies
877 [e.g., *Forest et al.*, 2008]. As a result of the respiration of
878 pelagic and benthic, terrigenous and marine organic matter,
879 the DIC in subsurface waters increases by $2.7\text{--}3.8\text{ mol C}$
880 $\text{m}^{-2}\text{ yr}^{-1}$ [*Renaud et al.*, 2007; *Richerol et al.*, 2008]. The

magnitude of benthic respiration is similar to the export rate
of terrigenous and marine organic matter from the subsur-
face layer. On the other hand, it should be stated that, given
the uncertainties of the budget terms, including the residence
time of the subsurface waters, we are presently unable to
determine if lateral inputs of either organic matter or
respired DIC to the study area are significant. It should also
be noted that, since we compiled data from different years,
our proposed budget reflects a climatological view rather
than a budget for any specific year.

4. Conclusions

[30] Dissolved Ba concentrations in the surface waters of
the Canadian Arctic Archipelago display only a slight sea-
sonality because the riverine inputs and the pulse in bio-
logical activity, which is accompanied by bio-Ba formation
and export, occur nearly simultaneously. Formation and
decay of bio-Ba shape the vertical nutrient-type profile of
dissolved Ba in our study area, but the contribution of
authigenic barite dissolution to the water column dissolved
Ba concentrations cannot be distinguished. We exploited
the seasonal Ba deficiency in the surface waters of the
Amundsen Gulf to estimate the particulate organic carbon
export out of the surface layer. This estimate, on the order
of $1.8 \pm 0.45\text{ mol C m}^{-2}\text{ yr}^{-1}$, allowed us to construct a
balanced carbon budget for the Amundsen Gulf. Within this
budget we identified and quantified relevant processes,
including the export of particulate organic carbon and its
subsequent respiration. Nevertheless, the role of lateral
carbon transport into and out of our study area remains to
be evaluated.

[31] **Acknowledgments.** We express our sincere gratitude to the
captains and crews who supported our work during the overwintering of
the CCGS Amundsen. We are grateful to those who helped us sample
for Barium and inorganic carbon parameters. This work is a contribution
to the Canadian IPY programs CFL and GEOTRACES, Swedish Research
Council, the Royal Society of Arts and Sciences, Swedish Research Council
project 2004–4034, to ArcticNet, as well as to the IGBP/IHDP core project
LOICZ. H. Thomas holds a Canada Research Chair. The manuscript greatly
benefited from the comments of two anonymous referees.

References

- Aristegui, J., S. Agustí, J. J. Middelburg, and C. M. Duarte (2005), Respiration in the mesopelagic and bathypelagic zones of the oceans, in *Respiration in Aquatic Ecosystems*, edited by P. A. del Giorgio and P. J. le B. Williams, pp. 181–205, Oxford Univ. Press, New York.
- Armstrong, R. A., M. L. Peterson, C. Lee, and S. G. Wakeham (2009), Settling velocity spectra and the ballast ratio hypothesis, *Deep Sea Res., Part II*, 56, 1470–1478, doi:10.1016/j.dsr2.2008.11.032.
- Arrigo, K. R., and G. L. van Dijken (2004), Annual cycles of sea ice and phytoplankton in Cape Bathurst polynya, southeastern Beaufort Sea, Canadian Arctic, *Geophys. Res. Lett.*, 31, L08304, doi:10.1029/2003GL018978.
- Bates, N. R., J. T. Mathis, and L. W. Cooper (2009), Ocean acidification and biologically induced seasonality of carbonate mineral saturation states in the Western Arctic Ocean, *J. Geophys. Res.*, 114, C11007, doi:10.1029/2008JC004862.
- Bishop, J. B. K. (1988), The barite-opal-organic carbon association in oceanic particulate matter, *Nature*, 332, 341–343, doi:10.1038/332341a0.
- Broecker, W. S., and T.-H. Peng (1982), *Tracers in the Sea*, 690 pp., Lamont-Doherty Geol. Obs., Palisades, N. Y.
- Buesseler, K. O. (1998), The de-coupling of production and particulate export in the surface ocean, *Global Biogeochem. Cycles*, 12, 297–310, doi:10.1029/97GB03366.
- Calvert, S. E., and T. F. Pederson (2007), Elemental proxies for palaeoclimatic and palaeoceanographic variability in marine sediments:

- 945 Interpretation and application, in *Proxies in the Late Cenozoic Paleoceanography*, edited by C. Hillaire-Marcel and A. de Vernal, pp. 567–644, Elsevier, Amsterdam, doi:10.1016/S1572-5480(07)01019-6.
- 948 Carmack, E. C., R. W. Macdonald, and S. Jasper (2004), Phytoplankton productivity on the Canadian Shelf of the Beaufort Sea, *Mar. Ecol. Prog. Ser.*, 277, 37–50, doi:10.3354/meps277037.
- 951 Chierici, M., A. Fransson, B. Lansard, L. A. Miller, A. Mucci, E. Shadwick, H. Thomas, J.-E. Tremblay, and T. N. Papakyriakou (2011), The impact of biogeochemical processes and environmental factors on the calcium carbonate saturation state in the Circumpolar Flaw Lead in the Amundsen Gulf, Arctic Ocean, *J. Geophys. Res.*, doi:10.1029/2011JC007184, in press.
- 957 Cooper, L. W., J. W. McClelland, R. M. Holmes, P. A. Raymond, J. J. Gibson, C. K. Guay, and B. J. Peterson (2008), Flow-weighted values of runoff tracers ($\delta^{18}\text{O}$, DOC, Ba, alkalinity) from the six largest Arctic rivers, *Geophys. Res. Lett.*, 35, L18606, doi:10.1029/2008GL035007.
- 961 Dehairs, F., W. Baeyens, and L. Goeyens (1992), Accumulation of suspended barite at mesopelagic depths and export production in the Southern Ocean, *Science*, 258, 1332–1335, doi:10.1126/science.258.5086.1332.
- 964 Dehairs, F., D. Shopova, S. Ober, C. Veth, and L. Goeyens (1997), Particulate barium stocks and oxygen consumption in the Southern Ocean mesopelagic water column during spring and early summer: Relationship with export production, *Deep Sea Res., Part II*, 44, 497–516, doi:10.1016/S0967-0645(96)00072-0.
- 969 Dehairs, F., N. Fagel, A. N. Antia, R. Peinert, M. Elskens, and L. Goeyens (2000), Export production in the Bay of Biscay as estimated from barium-barite in settling material: A comparison with new production, *Deep Sea Res., Part I*, 47, 583–601, doi:10.1016/S0967-0637(99)00072-2.
- 973 Dehairs, F., S. Jacquet, N. Savoye, B. A. S. van Mooy, K. O. Buesseler, J. K. B. Bishop, and C. H. Lamborg (2008), Barium in twilight zone suspended matter as a potential proxy for particulate organic carbon remineralization: Results for the North Pacific, *Deep Sea Res., Part II*, 55, 1673–1683, doi:10.1016/j.dsr2.2008.04.020.
- 978 Dickson, A. G., C. L. Sabine, and J. R. Christian (Eds.) (2007), *Guide to Best Practices for Ocean CO₂ Measurements*, *PICES Spec. Publ.*, vol. 3, 191 pp., North Pac. Mar. Sci. Org., Sidney, B. C., Canada.
- 981 Dymond, J., and R. Collier (1996), Particulate barium fluxes and their relationships to biological productivity, *Deep Sea Res., Part II*, 43, 1283–1308, doi:10.1016/0967-0645(96)00011-2.
- 984 Dymond, J., E. Suess, and M. Lyle (1992), Barium in deep-sea sediment: A geochemical proxy for paleoproductivity, *Paleoceanography*, 7, 163–181, doi:10.1029/92PA00181.
- 987 Else, B. G. T., T. N. Papakyriakou, R. J. Galley, W. M. Drennan, L. A. Miller, and H. Thomas (2011), Wintertime CO₂ fluxes in an Arctic polynya using eddy covariance: Evidence for enhanced air-sea gas transfer during ice formation, *J. Geophys. Res.*, 116, C00G03, doi:10.1029/2010JC006760.
- 992 Falkner, K. K., R. W. Macdonald, E. C. Carmack, and T. Weingartner (1994), The potential of barium as tracer of Arctic water masses, in *The Polar Oceans and Their Role in Shaping the Global Environment*, *Geophys. Monogr. Ser.*, vol. 85, edited by O. M. Johannessen, R. D. Muench, and J. E. Overland, pp. 63–76, AGU, Washington, D. C.
- 997 Forest, A., M. Sampei, R. Makabe, H. Sasaki, D. G. Barber, Y. Gratton, P. Wassmann, and L. Fortier (2008), The annual cycle of particulate organic carbon export in Franklin Bay (Canadian Arctic): Environmental control and food web implications, *J. Geophys. Res.*, 113, C03S05, doi:10.1029/2007JC004262.
- 1002 Forest, A., et al. (2011), Biogenic carbon flows through the planktonic food web of the Amundsen Gulf (Arctic Ocean): A synthesis of field measurements and inverse modeling analyses, *Prog. Oceanogr.*, doi:10.1016/j.pocean.2011.05.002, in press.
- 1006 Francois, R., S. Honjo, S. J. Manganini, and G. E. Ravizza (1995), Biogenic barium fluxes to the deep sea: Implications for paleoproductivity reconstruction, *Global Biogeochem. Cycles*, 9, 289–303, doi:10.1029/95GB00021.
- 1010 Gillikin, D. P., F. Dehairs, A. Lorrain, D. Steenmans, W. Baeyens, and L. André (2006), Barium uptake into shells of the common mussel (*Mytilus edulis*) and the potential for estuarine paleo-chemistry reconstruction, *Geochim. Cosmochim. Acta*, 70, 395–407, doi:10.1016/j.gca.2005.09.015.
- 1015 Guay, C. K., and K. K. Falkner (1997), Barium as tracer of Arctic halocline and river waters, *Deep Sea Res., Part II*, 44, 1543–1569, doi:10.1016/S0967-0645(97)00066-0.
- 1018 Guay, C. K., and K. K. Falkner (1998), A survey of dissolved barium in the estuaries of the major Arctic rivers and adjacent seas, *Cont. Shelf Res.*, 18, 859–882, doi:10.1016/S0278-4343(98)00023-5.
- 1021 Guay, C. K. H., F. A. McLaughlin, and M. Yamamoto-Kawai (2009), Differentiating fluvial components of upper Canada Basin waters on the basis of measurements of dissolved barium combined with other physical and chemical tracers, *J. Geophys. Res.*, 114, C00A09, doi:10.1029/2008JC005099.
- 1024 Hansell, D. A., D. Kadko, and N. R. Bates (2004), Degradation of terrigenous dissolved organic carbon in the western Arctic Ocean, *Science*, 304, 858–861, doi:10.1126/science.1096175.
- 1026 Hoppema, M., F. Dehairs, J. Navez, C. Monnin, C. Jeandel, E. Fahrback, and H. J. W. de Baar (2010), Dissolved barium distributions in the Weddell Gyre: Impact of circulation and biogeochemical processes, *Mar. Chem.*, 122, 118–129, doi:10.1016/j.marchem.2010.07.005.
- 1030 Horner, R., and G. C. Schrader (1982), Relative contributions of ice algae, phytoplankton and benthic microalgae to primary production in near-shore regions of the Beaufort Sea, *Arctic*, 35, 485–503.
- 1035 Jacquet, S. H. M. (2007), Barium in the Southern Ocean: Towards an estimation of twilight zone C mineralization, Ph.D. dissertation, 234 pp., Vrije Univ. Brussel, Brussels.
- 1037 Jacquet, S. H. M., F. Dehairs, D. Cardinal, J. Navez, and B. Dellile (2005), Barium distribution across the Southern Ocean frontal system in the Crozel-Kerguelen Basin, *Mar. Chem.*, 95, 149–162, doi:10.1016/j.marchem.2004.09.002.
- 1042 Jacquet, S. H. M., F. Dehairs, M. Elskens, N. Savoye, and D. Cardinal (2007), Barium cycling along WOCE SR3 line in the Southern Ocean, *Mar. Chem.*, 106, 33–45, doi:10.1016/j.marchem.2006.06.007.
- 1045 Juul-Pedersen, T., C. Michel, and M. Gosselin (2010), Sinking export of particulate organic material from the euphotic zone in the eastern Beaufort Sea, *Mar. Ecol. Prog. Ser.*, 410, 55–70, doi:10.3354/meps08608.
- 1048 Kellogg, C. T. E., S. D. Carpenter, A. A. Renfro, A. Sallon, C. Michel, J. K. Cochran, and J. W. Deming (2011), Evidence for microbial attenuation of particle flux in the Amundsen Gulf and Beaufort Sea: Elevated hydrolytic enzyme activity on sinking aggregates, *Polar Biol.*, doi:10.1007/s00300-011-1015-0, in press.
- 1051 Lanos, R. (2009), Circulation régionale, masses d'eau, cycles d'évolution et transports entre la mer de Beaufort et le golfe d'Amundsen, Ph.D. thesis, Univ. du Québec, Quebec, Canada.
- 1055 Lavoie, D., R. W. Macdonald, and K. L. Denman (2009), Primary productivity and export fluxes on the Canadian shelf of the Beaufort Sea: A modelling study, *J. Mar. Syst.*, 75, 17–32, doi:10.1016/j.jmarsys.2008.07.007.
- 1059 Macdonald, R. W., E. C. Carmack, F. McLaughlin, K. Iseki, D. Macdonald, and M. O'Brien (1989), Composition and modification of water masses in the Mackenzie shelf estuary, *J. Geophys. Res.*, 94, 18,057–18,070, doi:10.1029/JC094iC12p18057.
- 1062 Magén, C., G. Chailou, S. A. Crowe, A. Mucci, B. Sundry, A. Gao, R. Makabe, and H. Sasaki (2010), Origin and fate of particulate organic matter in the Southern Beaufort Sea—Amundsen Gulf region, Canadian Arctic, *Estuarine Coastal Shelf Sci.*, 86, 31–41, doi:10.1016/j.ecss.2009.09.009.
- 1066 Miller, L. A., T. N. Papakyriakou, R. E. Collins, J. W. Deming, J. K. Ehn, R. W. Macdonald, A. Mucci, O. Owens, M. Raudsepp, and N. Sutherland (2011), Carbon dynamics in sea ice: A winter flux time series, *J. Geophys. Res.*, 116, C02028, doi:10.1029/2009JC006058.
- 1072 Millero, F. J. (2006), *Chemical Oceanography*, 3rd ed., 531 pp., CRC Press, Boca Raton, Fla.
- 1073 Monnin, C. (1999), A thermodynamic model for the solubility of barite and celestine in electrolyte solutions and seawater to 200°C and 1 kbar, *Chem. Geol.*, 153(1–4), 187–209, doi:10.1016/S0009-2541(98)00171-5.
- 1077 Monnin, C., C. Jeandel, T. Cattaldo, and F. Dehairs (1999), The marine barite saturation state of the world's ocean, *Mar. Chem.*, 65, 253–261, doi:10.1016/S0304-4203(99)00016-X.
- 1080 Mucci, A., B. Lansard, L. A. Miller, and T. N. Papakyriakou (2010), CO₂ fluxes across the air-sea interface in the southeastern Beaufort Sea: The ice-free period, *J. Geophys. Res.*, 115, C04003, doi:10.1029/2009JC005330.
- 1084 Münchow, A., and H. Melling (2008), Ocean current observations from Nares Strait to the west of Greenland: Interannual to tidal variability and forcing, *J. Mar. Res.*, 66, 801–833.
- 1087 Mundy, C. J., et al. (2009), Contribution of under-ice primary production to an ice-edge upwelling phytoplankton bloom in the Canadian Beaufort Sea, *Geophys. Res. Lett.*, 36, L17601, doi:10.1029/2009GL038837.
- 1089 Papakyriakou, T., and L. A. Miller (2011), Springtime CO₂ exchange over seasonal sea ice in the Canadian Arctic Archipelago, *Ann. Glaciol.*, 52(57), 215–224, doi:10.3189/172756411795931534.
- 1091 Prange, M. (2002), Einfluss arktischer Süßwasserquellen auf die Zirkulation im Nordmeer und im Nordatlantik in einem prognostischen Ozean-Meereis-Modell, Ph.D. thesis, Univ. of Bremen, Bremen, Germany.
- 1096 Renaud, P. E., A. Riedel, C. Michel, N. Morata, M. Gosselin, T. Juul-Pedersen, and A. Chiuchiolo (2007), Seasonal variation in benthic community oxygen demand: A response to an ice algal bloom in the Beaufort Sea, Canadian Arctic?, *J. Mar. Syst.*, 67, 1–12, doi:10.1016/j.jmarsys.2006.07.006.

- 1102 Richerol, T., A. Rochon, S. Blasco, D. B. Scott, T. M. Schell, and R. J. 1145
 1103 Bennett (2008), Distribution of dinoflagellate cysts in surface sediments 1146
 1104 of the Mackenzie Shelf and Amundsen Gulf, Beaufort Sea (Canada), 1147
 1105 *J. Mar. Syst.*, 74, 825–839, doi:10.1016/j.jmarsys.2007.11.003. 1148
 1106 Semiletov, I., A. Makhtas, S.-I. Akasofu, and E. Andreas (2004), Atmo- 1149
 1107 spheric CO₂ balance: The role of Arctic sea ice, *Geophys. Res. Lett.*, 1150
 1108 31, L05121, doi:10.1029/2003GL017996. 1151
 1109 Shadwick, E. H., H. Thomas, Y. Gratton, D. Leong, S. Moore, T. N. 1152
 1110 Papakyriakou, and A. E. F. Prowe (2011a), Export of Pacific carbon 1153
 1111 through the Arctic Archipelago to the North Atlantic, *Cont. Shelf Res.*, 1154
 1112 31, 806–816, doi:10.1016/j.csr.2011.01.014. 1155
 1113 Shadwick, E. H., et al. (2011b), Seasonal variability of the inorganic carbon 1156
 1114 system in the Amundsen Gulf region of the southeastern Beaufort Sea, 1157
 1115 *Limnol. Oceanogr.*, 56, 303–322, doi:10.4319/lo.2011.56.1.0303. 1158
 1116 Sternberg, E., D. Tang, T.-Y. Ho, C. Jeandel, and F. M. M. Morel (2005), 1159
 1117 Barium uptake and adsorption in diatoms, *Geochim. Cosmochim. Acta*, 1160
 1118 69, 2745–2752, doi:10.1016/j.gca.2004.11.026. 1161
 1119 Sternberg, E., C. Jeandel, J.-C. Miquel, B. Gasser, M. Souhaut, R. Arraes- 1162
 1120 Mescoff, and R. Francois (2007), Particulate barium fluxes and export 1163
 1121 production in the northwestern Mediterranean, *Mar. Chem.*, 105, 281–295, 1164
 1122 doi:10.1016/j.marchem.2007.03.003. 1165
 1123 Sternberg, E., C. Jeandel, E. Robin, and M. Souhaut (2008), Seasonal cycle 1166
 1124 of suspended barite in the mediterranean sea, *Geochim. Cosmochim. 1167*
 1125 *Acta*, 72, 4020–4034, doi:10.1016/j.gca.2008.05.043. 1168
 1126 Taylor, J. R., K. K. Falkner, U. Schauer, and M. Meredith (2003), Quanti- 1169
 1127 tative considerations of dissolved barium as a tracer in the Arctic Ocean, 1170
 1128 *J. Geophys. Res.*, 108(C12), 3374, doi:10.1029/2002JC001635. 1171
 1129 Tremblay, J., K. Simpson, J. Martin, L. Miller, Y. Gratton, D. Barber, 1172
 1130 and N. M. Price (2008), Vertical stability and the annual dynamics of 1173
 1131 nutrients and chlorophyll fluorescence in the coastal, southeast Beaufort 1174
 1132 Sea, *J. Geophys. Res.*, 113, C07S90, doi:10.1029/2007JC004547. 1175
 1133 van Beek, P., E. Sternberg, J.-L. Reyss, M. Souhaut, E. Robin, and C. Jeandel 1176
 1134 (2009), ²²⁸Ra/²²⁶Ra and ²²⁶Ra/Ba ratios in the Western Mediterranean Sea: 1177
 1135 Barite formation and transport in the water column, *Geochim. Cosmochim. 1178*
 1136 *Acta*, 73, 4720–4737, doi:10.1016/j.gca.2009.05.063. 1179
 1137 Yamamoto-Kawai, M., and N. Tanaka (2005), Freshwater and brine behav- 1180
 1138 iors in the Arctic Ocean deduced from historical data of δ¹⁸O and alkali- 1181
 1139 nity (1992–2002 A.D.), *J. Geophys. Res.*, 110, C10003, doi:10.1029/ 1182
 1140 2004JC002793. 1183
 1141 Yamamoto-Kawai, M., F. A. McLaughlin, E. C. Carmack, S. Nishino, and 1184
 1142 K. Shimada (2008), Freshwater budget of the Canada basin, Arctic Ocean, 1185
 1143 from salinity, δ¹⁸O and nutrients, *J. Geophys. Res.*, 113, C01007, 1186
 1144 doi:10.1029/2006JC003858. 1187
- M. Chierici, Department of Chemistry, University of Gothenburg, 1157
 Kemiv. 10, SE-41296 Göteborg, Sweden. 1158
 F. Dehairs and J. Navez, Earth System Sciences and Analytical and 1159
 Environmental Chemistry, Vrije Universiteit Brussel, Pleinlaan 2, B-1050 1160
 Brussels, Belgium. 1161
 A. Fransson, Department of Earth Sciences, University of Gothenburg, 1162
 PO Box 460, SE-40530 Göteborg, Sweden. 1163
 Y. Gratton, INRS-EET, 490 de la Couronne, Quebec, QC G1K 9A9, 1164
 Canada. 1165
 B. Lansard and A. Mucci, Department of Earth and Planetary Sciences, 1166
 McGill University, 3450 University St., Montreal, QC H2A 3A7, Canada. 1167
 L. A. Miller, Institute of Ocean Sciences, Fisheries and Oceans Canada, 1168
 PO Box 6000, Sidney, BC V8L 4B2, Canada. 1169
 C. Monnin, Laboratoire Mécanismes et Transferts en Géologie, CNRS- 1170
 Université Paul Sabatier, F-31400 Toulouse, France. 1171
 T. N. Papakyriakou, Center for Earth Observation Science, University of 1172
 Manitoba, 470 Wallace Bldg., 125 Dysart Rd., Winnipeg, MB R3T 2N2, 1173
 Canada. 1174
 F. Prowe, Leibniz Institute of Marine Sciences at University of Kiel 1175
 (IFM-GEOMAR), Duesternbrooker Weg 20, D-24105, Kiel, Germany. 1176
 E. Shadwick, Antarctic Climate and Ecosystems Cooperative Research 1177
 Center, Hobart, TAS, Australia. 1178
 H. Thomas and E. Sternberg, Department of Oceanography, Dalhousie 1179
 University, 1355 Oxford St., Halifax, NS B3H 4J1, Canada. (helmuth. 1180
 thomas@dal.ca) 1181
 J.-É. Tremblay, Department de Biologie, Université Laval, Pavillon 1182
 Alexandre-Vachon, Quebec, QC G1V 0A6, Canada. 1183

Article